ACS APPLIED BIO MATERIALS

www.acsabm.org Article

3D Printed Angiogenin-Functionalized Bioresorbable Tubular Conduits for Biological Vascularization

Tanutrushna Sahoo,[#] Samir Das,[#] Sheeba Sonali, Sayan Mukherjee, Nantu Dogra, Chandrashish Roy, Radha Prabhu K, Sourabh Ghosh,* and Santanu Dhara*

Cite This: https://doi.org/10.1021/acsabm.5c02374 Read Online

ACCESS | Metrics & More | Article Recommendations | Supporting Information

ABSTRACT: Structural integrity of blood vessels is critical for maintaining physiological function *in vivo*. Damage or obstruction of capillaries and vessels that disrupt normal blood flow can lead to severe pathological conditions. Cardiovascular disorders such as atherosclerosis and aneurysms account for nearly 25% of total mortality. To address this clinical challenge, a bioresorbable tubular stent was fabricated using a composite ink of silk fibroin (SF) and gelatin methacrylate (GelMA), followed by surface functionalization with angiogenin cues. Rheological analysis of 15% SF-GelMA inks demonstrated shear-thinning behavior with a thermosensitive sol−gel transition. 3D-printed stents showed post-printing mechanical stability and compliance, exhibiting ∼0.45 MPa tensile strength with ∼17% elongation, thereby mimicking native soft vascular tissue under wet conditions. Following angiogenin functionalization, the resultant stents evidenced 20−25% bioresorbability over 15 days with low hemolysis (∼1%) and ∼45% higher cell viability *in vitro* over 5 days. Additionally, the computational modeling outcome of strong, stable binding between angiogenic proteins and activated SF-GelMA stent aligns with experimental outcomes. Overall, this study demonstrates potential of a 3D-printed, angiogenin-functionalized SF-GelMA tubular stent as a promising candidate for cardiovascular tissue regeneration, offering a synergistic combination of structural fidelity, biocompatibility, and pro-angiogenic activity.

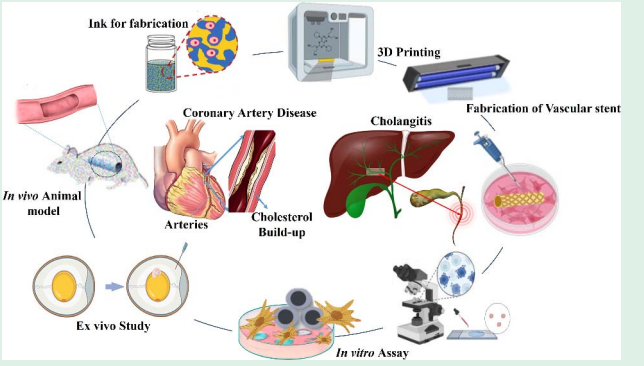

KEYWORDS: *silk fibroin, GelMA, 3D printing, angiogenic cues, tubular stent, ex vivo and in vivo study*

Downloaded via INDIAN INST OF TECH DELHI- IIT on June 12, 2026 at 13:47:25 (UTC).
See https://pubs.acs.org/sharingguidelines for options on how to legitimately share published articles.

1. INTRODUCTION

Human body depends on a network of biological conduits to transport essential fluids and sustain vital physiological functions. Cardiovascular diseases (CVDs) represent a significant global health burden, accounting for over 17 million deaths annually, according to the World Health Organization (WHO).[1] Conditions such as atherosclerosis and aneurysms compromise vascular integrity, potentially leading to myocardial infarction, stroke, or fatal hemorrhage.[2,3] Despite the widespread use of surgical reconstruction with autologous grafts for bypass surgeries, their application is frequently limited by donor site morbidity and restricted availability, particularly in patients with extensive vascular disease.[4,5] Metallic stents initially offered effective structural support; however, their long-term use was limited by complications such as restenosis, thrombosis, in-stent fractures, structural degradation, and inflammatory responses triggered by ion release and corrosion.[6,7] Synthetic blood vessels present a potential alternative due to their immediate availability; however, they are often associated with poor biocompatibility and inadequate integration with host tissues, which can lead to thrombosis or infection.[8] Therefore, the successful implementation of graft-based therapies requires a comprehensive understanding of the tissue microenvironment, mechanical compatibility, and host immune response.

Polymer-based tubular conduits, such as Dacron[9] and expanded PTFE,[10] face significant limitations, particularly poor long-term patency in small-diameter vessels (<6 mm).[11,12] Nylon is promising in the early days of implantation, but rapid degradation limits its durability,[13] whereas expanded PTFE shows comparable patency rates but underperforms over time under *in vivo* conditions.[14,15] Polyurethane (PU) stents exhibit better resistance to thrombosis, support fibrous tissue ingrowth,[16] have low mechanical strength, and show inconsistent degradation under physiological conditions,[17] which limits their specific application (i.e., vascular vs ureteral). Biodegradable polymeric stents like PCL and PGLA can enhance cell adhesion and pro-

Received: November 28, 2025
Revised: March 3, 2026
Accepted: March 5, 2026

ACS Publications © XXXX American Chemical Society

liferation,[18,19] but their clinical potential is limited by hydrophobicity, low bioactivity, and slow degradation rate.[20] This underscores the need for advanced biomaterials that not only exhibit biocompatibility and mechanical robustness but also promote cell adhesion, proliferation, and functional tissue regeneration.

Silk fibroin (SF) offers significant biocompatibility,[21] biodegradability,[22] and ECM-like properties[23] conducive to endothelial and smooth muscle cell growth under arterial conditions,[24] especially after sericin removal.[25] GelMA provides tunable stiffness and cell-adhesive properties,[26] while their combination enhances mechanical strength, printability, and bioactivity.[27] Composite hydrogel consisting of silk fibroin (SF) and gelatin methacrylate (GelMA) can overcome these limitations. Angiogenin (Ang) is widely recognized for its pro-angiogenic function, which poses significant concerns when its expression becomes dysregulated. Elevated levels of Ang have been implicated in pathological angiogenesis, leading to accelerated tumor growth and cancer progression. This has been demonstrated in recent studies utilizing 3D tumor angiogenesis models, which serve as physiologically relevant platforms to investigate complex interactions between endothelial cells and tumor cells.[28] The role of endothelial-associated proteins such as T-cadherin in regulating tumor-driven vascularization has been highlighted through studies using multicellular tumor spheroid models.[29] Additionally, certain Ang mutations have been associated with neurodegenerative disorders such as amyotrophic lateral sclerosis (ALS) and Parkinson's disease, emphasizing the importance of tightly regulating its biological activity. To overcome these limitations, this project employs a controlled and localized delivery approach for Ang within bioengineered vascular stents, leveraging computational modeling studies to optimize Ang binding to the EDC/NHS-activated hydrogel matrix. By confining Ang activity to the stent site, the strategy promotes site-specific angiogenesis, supporting neovascularization without triggering systemic side effects linked to uncontrolled Ang expression. Further, incorporating angiogenic factors such as Ang is expected to improve vascularization[30] and biological mimicry for small-diameter vascular stents that support endothelialization, cell proliferation, and functional tissue regeneration.[31,32] This targeted approach addresses the longstanding challenge of poor vascular integration in tissue-engineered constructs, offering a promising solution for enhancing graft performance and long-term clinical success.

In the present study, 3D printing technique was employed to fabricate a tubular stent using a composite ink that combines the mechanical robustness of silk with biologically active GelMA, along with covalently bound angiogenin to specifically target small-diameter vascular regeneration. Notably, both protein components differ in biodegradability. Molecular modeling studies supported the stability, enhanced protein retention, and bioactivity of angiogenin incorporation within the SF-GelMA matrix. Characterization methods such as NMR and ninhydrin assays confirmed successful methacrylation, resulting in improved UV crosslinking efficiency post-printing. Mechanical testing demonstrated suitable elasticity and tensile strength, supporting its application in small-diameter vascular reconstructions. Swelling and degradation analysis, along with biological assays, indicated cytocompatibility for SF-GelMA-angiogenin tubular stents for improved tissue integration. These findings were further validated through subcutaneous implantation in a rat model and *ex vivo* studies using the chorioallantoic membrane (CAM) assay.

2. MATERIALS AND METHODS

2.1. Materials

Bombyx mori silk cocoons were procured from Central Silk Board, Bangalore. Chemical compounds such as sodium carbonate (Na_2CO_3), lithium bromide (LiBr), gelatin powder of porcine origin (Type A, bloom number 300 g), Irgacure 2959, deuterium oxide (D_2O), pepsin, methacrylic anhydride (MA), 1-ethyl-3-(3-dimethylaminopropyl) carbodiimide (EDC), *N*-hydroxysuccinimide (NHS), 6-diamidino-2-phenylindole, dihydrochloride (DAPI), and rhodamine phalloidin (RP) were obtained from Sigma-Aldrich. Dialysis membranes (SnakeSkin 3.5 K and 10 K MWCO dialysis tubing) and the BCA Protein Assay Kit were purchased from Thermo Fisher Scientific, USA. Cell culture media and dyes, including MTT powder (dimethylthiazol-diphenyltetrazolium bromide, Sigma, St. Louis, USA), DMEM low-glucose medium (Gibco, Life Technologies, USA), 0.05% trypsin−EDTA solution (Gibco, USA), fetal bovine serum (FBS) (Gibco, USA), and Live/Dead Assay Kit (Life Technologies, USA) were sourced from various suppliers.

2.2. Computational Modeling Analysis

The three-dimensional crystallographic coordinates of SF were obtained from the Protein Data Bank (PDB ID: 3UA0) and served as the structural backbone for hydrogel modeling. This protein was selected due to its biocompatibility, mechanical strength, and widespread use in scaffold-based tissue engineering. Angiogenesis-related target proteins, namely, VEGF (PDB ID: 2VPF) and Ang (PDB ID: 1ANG), were also retrieved from the PDB in their experimentally resolved, high-resolution forms. The chemical structures of the carbodiimide crosslinking reagents EDC (PDB Ligand ID: EDC) and NHS (PDB Ligand ID: NHS) were similarly acquired from the PDB ligand database. Since no crystallographic or computational models of GelMA were available in public repositories, the GelMA monomer was constructed de novo in ChemDraw based on the known chemical modification of gelatin through methacrylic anhydride targeting lysine residues. The ChemDraw generated GelMA structure was exported in MOL format, converted to PDB format, and energy-minimized prior to docking. All structures were prepared for subsequent simulations, with figure color coding assigned consistently with Figure 1A−C: SF (green), EDC/NHS (red), GelMA (blue), VEGF (orange), Ang (magenta), and hydrophobic interaction zones (yellow). All protein and ligand structures were first processed to ensure compatibility for docking studies. Protein preparation involved the removal of crystallographic water molecules, heteroatoms, and redundant chain segments, followed by addition of polar hydrogens and assignment of Kollman charges. Energy minimization of the proteins was performed using the AMBER ff14SB force field to resolve steric clashes and optimize side-chain orientations. Ligands (EDC, NHS, and GelMA) were prepared by optimizing their geometries using the GAFF force field, with torsional flexibility retained to allow realistic binding conformation sampling. The first stage of docking involved ligand−ligand interaction modeling between GelMA and EDC to form the reactive O-acylisourea intermediate, followed by the introduction of NHS to simulate the formation of the more stable NHS-ester. This step mimicked the carbodiimide chemistry used experimentally for hydrogel crosslinking. AutoDock Vina was used for these simulations, with an exhaustiveness parameter of 32 to ensure adequate conformational space sampling. The resulting EDC/NHS-activated GelMA model was then spatially positioned on the SF structure to generate the SF-GelMA-EDC/NHS composite hydrogel model. For protein hydrogel interactions, both VEGF and Ang were docked to the hydrogel model using a blind docking approach that encompassed the entire surface of the SF-GelMA-EDC/NHS structure. The docking grid dimensions were adjusted to fully cover the composite, ensuring unbiased sampling of potential binding sites. ClusPro scoring was applied to evaluate the binding poses, with the best complexes identified based on the lowest C-scores and minimal RMSD values (<0.3 Å) between pose clusters. All binding modes were visualized and analyzed using UCSF

https://doi.org/10.1021/acsabm.5c02374
ACS Appl. Bio Mater. XXXX, XXX, XXX−XXX

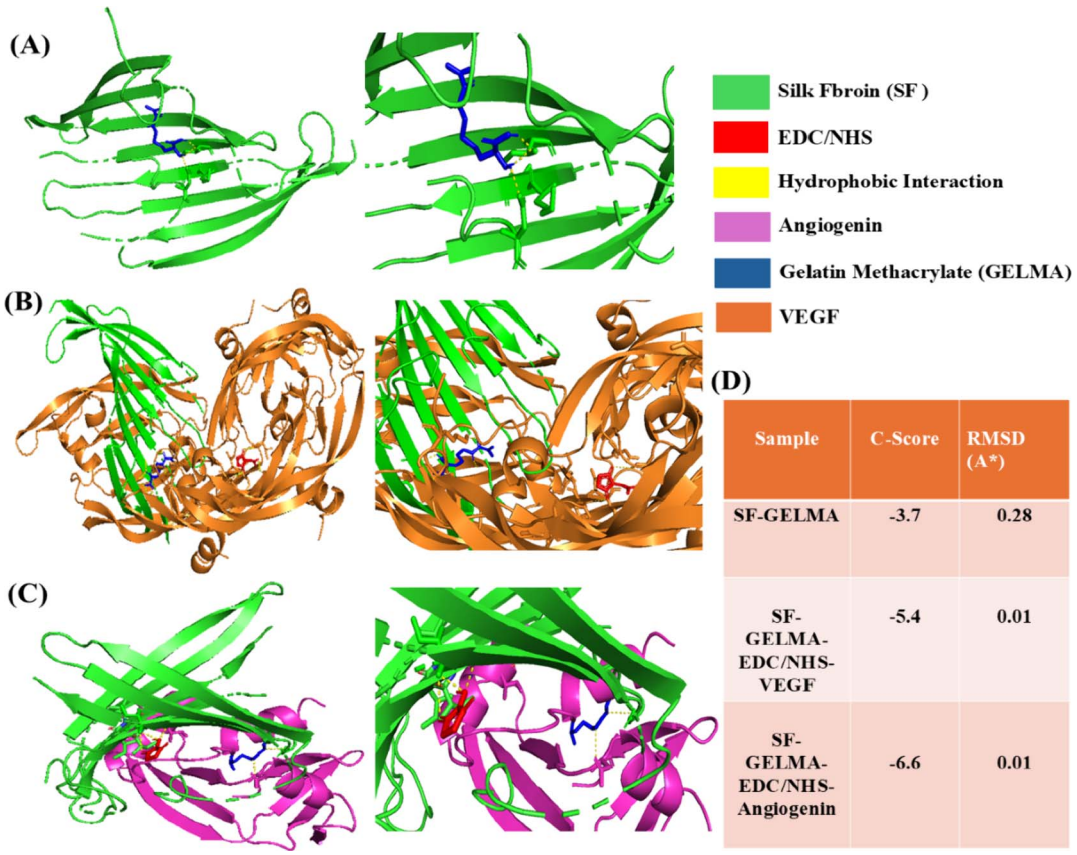

(D)

Sample	C-Score	RMSD (A*)
SF-GELMA	-3.7	0.28
SF-GELMA-EDC/NHS-VEGF	-5.4	0.01
SF-GELMA-EDC/NHS-Angiogenin	-6.6	0.01

Figure 1. (A–C) Computational modeling configurations illustrating interaction modes of unmodified SF-GelMA and EDC/NHS activated SF-GelMA with angiogenin and VEGF. (D) Docking analysis identified angiogenin as the strongest binder in EDC/NHS activation, with the lowest C-score demonstrated the strongest binding affinity.

Chimera, PyMOL, and Discovery Studio Visualizer. Interaction types, including hydrogen bonding, hydrophobic contacts, and π–π stacking, were mapped for each complex, with specific zones of hydrophobicity highlighted in yellow for visual clarity.

2.3. Preparation of Silk Fibroin (SF) Solution

The SF solution from *Bombyx mori* cocoons was prepared as described previously.[33,34] SF was extracted from raw silk cocoons by first degumming 5 g of silk in 0.02 M sodium carbonate (Na_2CO_3) solution at elevated temperatures, followed by rinsing and overnight drying. The dried silk fibers were dissolved in 9.3 M lithium bromide (LiBr) solution in a 1:4 ratio at 60 °C for 4 h. The solution was dialyzed for 48 h using a 3.5 kDa membrane to remove the LiBr and centrifuged for 10 min at 4 °C to remove any remaining impurities.

2.4. Synthesis of Gelatin Methacrylate (GelMA)

Gelatin was dissolved in PBS at 50 °C for 20 min at a concentration of 10 w/v %. Methacrylic anhydride was then added dropwise into the solution along with constant stirring at 50 °C. The methacrylation reaction was allowed to proceed for 3 h under continuous stirring. After the reaction, the solution was centrifuged in a Falcon tube at 1000*g* for 2 min to eliminate any excess methacrylic anhydride. The supernatant was collected and dialyzed against distilled water for 4–5 days at 50 °C. Following the dialysis, the pH of the solution was adjusted to 7.0–7.4, and the product was transported to 50 mL Falcon tubes. The GelMA was frozen at −80 °C overnight and subsequently lyophilized for a week, as depicted in Figure 2A, for further use.[35]

2.5. Spectroscopy Analysis and Degree of Methacrylation of GelMA

Fourier transform infrared (FTIR) spectroscopy was conducted (Model: M/S, Thermo Fisher Scientific Instruments, USA) to characterize the chemical structure of gelatin and gelatin methacryloyl (GelMA) in the wavenumber range of 400–4000 cm^{-1} with a resolution of 4 cm^{-1}. A total of 32 scans were recorded per sample. The successful incorporation of methacrylamide and methacrylate functional groups in the GelMA structure was confirmed through characteristic absorption peaks observed in the FTIR spectrum.[36]

Further, NMR spectroscopy was performed to analyze and compare the chemical structures of gelatin and GelMA.[37] Both samples were dissolved in deuterated water (D_2O) at a concentration of 10 mg/mL. The clear solutions were then transferred to NMR tubes and analyzed at room temperature using a 400 MHz NMR spectrometer. Chemical shifts were recorded in parts per million (ppm), with the solvent peak at $\delta = 4.79$ ppm for D_2O serving as the reference. The NMR data were post-processed using MestReNova software to identify characteristic peaks and evaluate structural modifications. The degree of methacrylation (DoM) was quantitatively assessed by comparing peak intensities, as described in previous studies,[38] and further validated through a ninhydrin assay.

2.6. Ninhydrin Assay

The standard curve of gelatin solution was diluted to concentrations ranging from 1 to 10 mg/mL. GelMA samples were prepared at a concentration of 10 mg/mL in 1 mL of PBS, while ninhydrin solution was prepared at 2.5 mg/mL in 100% ethanol. Each 400 μL sample was

https://doi.org/10.1021/acsabm.5c02374
ACS Appl. Bio Mater. XXXX, XXX, XXX–XXX

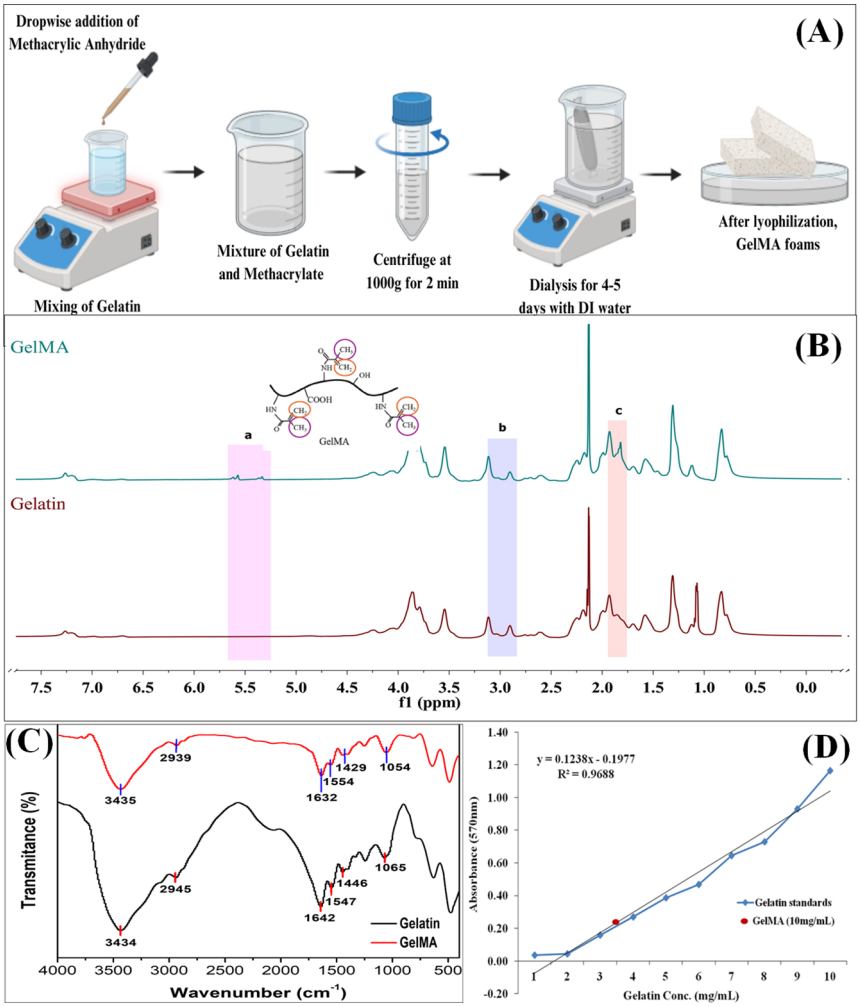

Figure 2. GelMA synthesis and physicochemical characterizations. (A) Schematic process of the preparation of GelMA; (B) ^{1}H-NMR spectra evidence the DoM of gelatin and GelMA; (C) FTIR spectra for functionalized group determination standard; (D) standard curve of gelatin generated for the ninhydrin assay.

combined with 50 μL of ninhydrin solution and incubated in a 70 °C hot air oven for 1 h. After incubation, optical absorbance was measured at 570 nm. The DoM of GelMA was calculated as (100−X) %, where X is GelMA's absorbance value on the gelatin standard curve with an R^2 value of 0.9688.

2.7. Preparation of SF-GelMA Ink

Irgacure 2959 of 0.5 w/v % was added to a 7.5 w/v % silk fibroin solution for preparing the printable ink. GelMA foams were dispersed in that SF-Irgacure 2959 solution at varied concentrations of 10, 15, and 20 w/v % to control the viscosity of the precursor solution. This suspension was heated at 40−45 °C for 30 min. The ink was then centrifuged in a mini centrifuge for 5 min to remove the voids. Finally, the ink was loaded into a syringe and tested for printability, considering the gelation time.

2.8. Rheological Analysis of SF-GelMA Ink

Rheological characterization was carried out to assess the printability and flow behavior of SF-GelMA inks formulated with varying concentrations of GelMA (10%, 15%, and 20% w/v). All measurements were performed using a rotational rheometer (Anton Paar, Physica MCR 302) equipped with a parallel plate geometry (PP35/TG) and a fixed gap of 1 mm. Shear-thinning behavior was investigated by measuring viscosity as a function of shear rate ranging from 1 to 100 s^{-1} at a constant temperature of 25 °C.[38] In addition, temperature-dependent viscosity profiles were obtained for each formulation over a temperature range of 10 °C to 40 °C at a constant shear rate.[39] During temperature sweep experiments, the storage modulus (G') and loss modulus (G'') were recorded from 10 °C to 40 °C at a constant angular frequency of 10 rad/s and 1% strain, ensuring that measurements remained within the linear viscoelastic region. Additionally, frequency sweep tests were conducted at 25 °C over a range of 0.1 to 100 rad/s using the same strain amplitude.[40]

2.9. Design and Fabrication of the 3D Printed Tubular Stent

The customized hierarchy of the tubular stent was developed using computer-aided design (CAD) in SolidWorks (version 2020 SP4, Dassault Systèmes SolidWorks Corp.). The.stl file was processed in CURA (v15.04.5, Ultimaker) and converted into GCODE with optimized printing parameters based on the rheological study of the ink. The GCODE file was imported into an extrusion-based 3D printer

https://doi.org/10.1021/acsabm.5c02374
ACS Appl. Bio Mater. XXXX, XXX, XXX−XXX

(Alfatek Systems, India), and printing was performed using the rotating Spindle mode. The tubular stent was fabricated using SF-GelMA ink, which was loaded into 5 mL UNO-LOCK syringes without much void entrapment. Printing was performed at 4 °C with a flow rate of 2 mL/min using a 600 μm nozzle diameter. The printed constructs were first stabilized at 4 °C to allow physical gelation, followed by UV light exposure to initiate photopolymerization and achieve complete crosslinking. The Irgacure 2959 decomposes to generate free radicals under UV exposure, which trigger crosslinking between methacrylate groups on the GelMA chains. This results in the formation of a stable, covalently crosslinked hydrogel network in the printed structure. Final stents were stored in PBS at 37 °C to assess structural integrity.

2.10. Physicochemical Characterization of the Tubular Stent

The nature of chemical bonds and molecular interactions within the fabricated SF-GelMA tubular stent was investigated using FTIR spectroscopy. To determine the crystalline nature of the individual constituents and the composite construct, X-ray Diffraction (XRD) analysis was conducted utilizing a Bruker A25 diffractometer (Bruker, Germany) equipped with a Cu Kα radiation source (λ = 1.5406 Å). The diffraction patterns were recorded over a 2θ range of 10° to 80° using an optimized step size to ensure high-resolution data acquisition for phase identification and crystallinity assessment.

2.11. Mechanical Properties

The mechanical properties of the 3D-printed SF-GelMA tubular stents were evaluated for both wet (swelling in PBS) and dry samples based on ASTM D638 standard using a Universal Testing Machine (UTM, model H25KS; Hounsfield, UK) equipped with a 100 N load cell. The tensile test with a maximum capacity of 100 N was done until the point of rupture. The stress−strain behavior of the samples was recorded in real time, from which tensile strength and elongation at break were determined. All tests were performed in triplicate to ensure reproducibility.

2.12. Incorporation of the Angiogenic Factor with Physicochemical Characterization

The vascularization and endothelialization potential of the fabricated SF-GelMA tubular stent was enhanced by incorporating angiogenin cues using carbodiimide chemistry. The interaction mechanism relies on the activation of free carboxyl groups (−COOH) present on the aspartic and glutamic acid residues of the SF and GelMA backbone. The carboxyl groups of printed stents were activated by immersing in 20 mM EDC solution for 3 h. This produced a reactive O-acylisourea intermediate. This intermediate was subsequently stabilized by the addition of 20 Mm NHS solution for 3 h,[41] converting it into a semi-stable NHS-ester. 70 ng/mL angiogenic solution was then added to the mixture and incubated for 12 h at 37 °C. During this process, the primary amine groups ($-NH_2$) on the lysine residues of the angiogenin protein performed a nucleophilic attack on the NHS-esters. This conjugation resulted in the formation of robust, covalent amide (peptide) bonds, effectively anchoring the angiogenic factor to the hydrogel matrix. After conjugation, stents were kept at 4 °C for 3 h and air-dried under sterile conditions. This method allowed for the covalent immobilization of angiogenin onto the stents, potentially promoting angiogenesis upon implantation.

Field emission scanning electron microscopy (FESEM) (Model: Gemini 300, ZEISS Co.), coupled with energy dispersive X-ray spectroscopy (EDX), was employed for the morphological and elemental characterization of both SF-GelMA and angiogenin-functionalized SF-GelMA (SF-GelMA-Ang) tubular stent. X-ray photoelectron spectroscopy (XPS) was conducted using a PHI 5000 VERSA PROBE III system (ULVAC PHI, USA), equipped with a monochromatic Al Kα source, to examine the surface elemental composition and chemical states before and after angiogenin conjugation. The successful covalent crosslinking of angiogenin was further confirmed by FTIR analysis. Further, Fourier self-deconvolution (FSD) spectra were generated using Origin 2021, which revealed distinct functional group signatures associated with the successful conjugation.

2.13. Swelling Assay

The swelling behavior of SF-GelMA and SF-GelMA-Ang tubular stents was systematically evaluated. Each stent sample (in triplicate) of equal weight was immersed in PBS (pH 7.4) at 37 °C for 2, 4, 6, 8, 12, and 24 h. After incubation, samples were gently blotted to remove surface moisture, and the swollen weights were recorded to assess water uptake of samples incubated for different durations.[42]

$$\text{Swelling Ratio, S}(\%) = \frac{WT_f - WT_i}{WT_i} \times 100 \quad (1)$$

where WT_f is the final weight after swelling and WT_i is the initial dried sample weight.

2.14. Protein Adsorption Study

Protein adsorption was measured for SF-GelMA and SF-GelMA-Ang tubular stents by immersing equal weight samples in 300 μL of 0.1% BSA solution (PBS, pH 7.4) at 37 °C for 2−24 h. The bicinchoninic acid (BCA) protein assay was performed to quantify the amount of protein adsorbed onto the stent surface. The working solution was prepared by mixing the BCA reagent with a 4% (w/v) copper(II) sulfate pentahydrate solution in a 50:1 ratio. This reagent mixture was added to each sample and incubated for 3 h at 37 °C to allow for color development. After incubation, the absorbance of each sample was measured at 570 nm using a microplate reader.[43]

2.15. *In Vitro* Degradation Assay

The degradation behavior of SF-GelMA and SF-GelMA-Ang tubular stent was assessed under physiological (PBS) and enzymatic (PBS with 1 mg/mL pepsin) conditions. Uniformly cut, pre-weighed dry samples were incubated at 37 °C for 15 days in both media. At intervals of 3 days, samples were retrieved from each group for analysis. The samples were then placed in a vacuum oven for 12 h before being measured for their final weight.

$$\text{Rate of degradation, D}(\%) = \frac{W_i - W_f}{W_i} \times 100 \quad (2)$$

where W_i is the initial captured dried weight at the start before immersing the stent and W_f is the final weight.[18]

2.16. Hemocompatibility Assay

The hemocompatibility of SF-GelMA and SF-GelMA-Ang tubular stent was assessed by conducting a hemolysis assay. Red blood cells (RBCs) were isolated by centrifugation of human blood collected in EDTA-containing tubes. The isolated RBCs were washed thoroughly with PBS to remove plasma proteins and other residual components. Subsequently, the RBCs were diluted in PBS at a ratio of 1:5 (v/v) for preparing a working stock of RBC suspension. Sterilized stents of equal dimensions were incubated in the RBC suspensions at 37 °C for 3 h. After post-incubation, absorbance was measured at 545 nm with water as a positive control and PBS as a negative control.[44] The percentage of hemolysis was calculated using the following formula:

$$\text{Hemolysis}(\%) = \frac{A_{sample} - A_{NC}}{A_{PC} - A_{NC}} \times 100 \quad (3)$$

where A_{sample}, A_{NC}, and A_{PC} represent the absorbance values of the test sample, negative control, and positive control, respectively.

Furthermore, RBC morphology over the sample surface was analyzed using SEM to observe erythrocyte adhesion and morphology over the surface of both stent types.

https://doi.org/10.1021/acsabm.5c02374
ACS Appl. Bio Mater. XXXX, XXX, XXX−XXX

2.17. *In Vitro* Cytocompatibility Assay of Tubular Stents

As per ISO 10993-5, the L929 fibroblast cell line was employed for cytocompatibility testing, including cell proliferation and morphological analysis. Their established sensitivity to cytotoxic agents and reproducibility in interlaboratory comparisons supported their application for robust cytocompatibility testing of the developed materials.

2.17.1. Cell Proliferation Assessment. The cytocompatibility of SF-GelMA and SF-GelMA-Ang tubular stents was assessed using the MTT assay with L929 fibroblast cells. Sterilized 0.5 cm stents were placed in a 48-well tissue culture plate, and 50,000 cells/well were seeded to ensure uniform coverage on inner and outer surfaces. Cells were cultured in Dulbecco's modified Eagle medium (DMEM) with 10% FBS and 1% penicillin−streptomycin at 37 °C in a humidified atmosphere with 5% CO_2 for 1, 3, and 5 days. At each time point, MTT solution (0.5 mg/mL in serum-free DMEM) was replaced with culture medium and incubated in the dark at 37 °C for 4 h. Formed formazan crystals were then dissolved in 200 μL of DMSO, and absorbance was measured at 570 nm to quantify cell viability. To calculate the final cell viability, we used the following formula:[45]

$$\text{Cell viability}(\%) = \frac{G_{abs} - B_{abs}}{C_{abs} - B_{abs}} \times 100 \quad (4)$$

where G_{abs} is the absorbance of the stent with cells, B_{abs} is the blank absorbance, and C_{abs} is the absorbance of the control well (TCPS).

2.17.2. Live-Dead Assay and Morphological Analysis. Live/dead staining was performed to qualitatively assess the cell viability of L929 on both SF-GelMA and SF-GelMA-Ang tubular stents, in which TCP served as the control. After 1, 3, and 5 days of incubation, the samples ($n = 3$) were stained using calcein-AM and ethidium homodimer-1, following the manufacturers' instructions. The stained constructs were incubated at 37 °C in the dark for 30 min, followed by imaging under a fluorescence microscope (Axio Observer, Carl Zeiss, Germany). SF-GelMA-Ang tubular stents were fixed in 4% paraformaldehyde after 1, 3, and 5 days of *in vitro* culture, permeabilized with a 0.1% Triton X-100 solution, and subsequently washed multiple times with PBS (pH 7.4). This was followed by staining with rhodamine phalloidin (Invitrogen) and 4′,6-diamidino-2-phenylindole (DAPI; Invitrogen) according to the manufacturer's protocol. Fluorescence microscopy was performed with an Axio Observer Z1 microscope (Carl Zeiss) to capture the images of the samples. For morphological evaluation, cell-seeded samples were subjected to dehydration using a gradient of isopropanol solutions (60−100%) and subsequently examined via scanning electron microscopy (SEM).

2.18. *Ex Vivo* Evaluation Using the Chorioallantoic Membrane Assay (CAM)

The angiogenic potential of the developed SF-GelMA and SF-GelMA-Ang tubular stents was assessed by performing a chorioallantoic membrane (CAM) assay. Fertilized duck eggs were incubated at 37 °C and 80% relative humidity for 5 days. On embryonic day 6, the eggs were removed from the incubator, gently cleaned with 70% ethanol to ensure sterilization, and a small window (~1 cm^2) was created on the air sac side of each egg using sterilized tweezers to access the CAM. Sterile pieces (3−5 mm) of SF-GelMA and SF-GelMA-Ang tubular stents were gently placed on the exposed CAM surface. A control group without any material was maintained for comparison. Based on study time, the CAMs were imaged, and the degree of neovascularization was assessed by quantifying the number of blood vessels converging toward the stent using ImageJ software.

2.19. *In Vivo* Subcutaneous Implantation

All procedures were performed per the Council's guidelines to control and supervise experiments on animals (CPCSEA), Government of India, following Helsinki guidelines. Adult male Wistar rats (150−200 g, 8−9 weeks old) were purchased from the CPCSCA Registered Lab (reg no 1828/PO/Bt/S/15/CPCSCA, under the Min of Environment Welfare Div, GOI) and maintained in the animal house with controlled humidity and temperature under alternative light−dark cycle conditions. Ethical clearance was obtained from the Institutional Animal Ethics Committee (IAEC) at the Indian Institute of Technology, Kharagpur (Protocol No. IE-02/SD-SMST/2.22), in accordance with CPCSEA and NIH animal care regulations.

Tubular stents of SF-GelMA and SF-GelMA-Ang were 1.5 cm in length and 4 mm in luminal width were embedded, as per the operational procedure mentioned by Tseng et al.[46] The stent study was conducted for 21 days (in triplicate); the stents were placed subcutaneously under anesthesia (intramuscular injection (xylazine (5 mg/kg) and ketamine hydrochloride (20 mg/kg), 3% isoflurane), as reported by Ojha et al.[47] Next, a 2 cm cut was made using a scalpel to embed the stents into the dorsal subcutaneous pouches of the rats. Postoperative care included local antiseptic application and regular monitoring for inflammation, infection, or any abnormal behavior throughout the recovery period. After 21 days, the rats were anesthetized to harvest the stents with surrounding connective tissue and were fixed in neutral buffered formalin (Merck, USA). It was processed further for paraffin embedding for histopathological studies using hematoxylin & eosin (H&E, Merck, USA) and Masson's Trichome kit (Sigma-Aldrich, USA) following the manufacturer's instructions. Major organs of the implanted animals were obtained, and optical images were taken to evaluate the safety/toxicity of implanted stents.

2.20. Histological Analysis

The retrieved specimens were preserved in 4% paraformaldehyde, dehydrated through a gradient of ethanol solutions (50−100%) and xylene, and subsequently embedded in paraffin for histological sectioning. Sections were extracted from the paraffin blocks utilizing a microtome (Leica RM2125 RTS, Germany), and staining was performed with Hematoxylin and Eosin (H&E) and Masson trichrome (MT) to examine the tissue architecture in the SF-GelMA and SF-GelMA-Ang samples. Histological samples were photographed post-staining with an Axio Observer Z1 microscope.

2.21. Statistical Analysis

The disparities between the experimental group and control group were analyzed by conducting statistical analysis. One-way analysis of variance (ANOVA) of the groups to understand the overall variation was performed. It was followed by a *t*-test conducted in GraphPad Prism software (version 5.02) to identify the specific differences. The significance level was determined as $p < 0.05$.

3. RESULTS AND DISCUSSION

3.1. Computational Modeling of Growth Factor Interactions with Cross-Linked SF-GelMA

The computational docking studies revealed distinct binding profiles for SF-GelMA, SF-GelMA-EDC/NHS, and their complexes with angiogenic proteins. In the unmodified hydrogel system (Figure 1A), GelMA (blue) was observed to bind along the surface-exposed β-sheet domains of SF (green) through multiple hydrogen bonds and localized hydrophobic patches (yellow). This configuration resulted in a C-score of −3.7 and an RMSD of 0.28 Å, indicating a moderately stable complex with a consistent binding orientation across docking replicates. When angiogenin (magenta) was introduced to the EDC/NHS-activated SF GelMA complex (Figure 1C), the docking simulations demonstrated a markedly stronger interaction. The EDC/NHS moieties (red) formed additional hydrogen bonds with polar residues on angiogenin, while GelMA's methacryloyl groups engaged in hydrophobic stabilization. This dual interaction mechanism involved covalent crosslinking simulation via EDC/NHS and

https://doi.org/10.1021/acsabm.5c02374
ACS Appl. Bio Mater. XXXX, XXX, XXX−XXX

secondary hydrophobic contacts. It produced a significantly improved C-score of −6.6. The RMSD was exceptionally low at 0.01 Å. These results reflect both strong binding affinity and high conformational reproducibility. Similarly, VEGF (orange) docking to the EDC/NHS-activated SF-GelMA (Figure 1B) revealed extensive hydrogen bonding and aromatic interactions at the protein−hydrogel interface. Notably, the NHS ester regions interacted with lysine rich patches on VEGF, while the methacryloyl modified gelatin contributed hydrophobic pocket stabilization. This configuration yielded a C-score of −5.4 and an RMSD of 0.01 Å, again suggesting strong affinity with minimal pose variation between runs.

The docking performance metrics are shown in Panel D, highlighting a clear trend: incorporation of EDC/NHS activation significantly enhanced both C-score and RMSD stability compared to the unmodified SF GelMA system. Between the two angiogenic targets, angiogenin exhibited the most favorable binding parameters, suggesting that it may have a stronger thermodynamic compatibility with the EDC/NHS activated hydrogel based stent. These findings confirm that carbodiimide mediated activation of GelMA in an SF matrix substantially increases the stability and strength of protein binding, a factor that may translate into improved bioactivity in tissue engineering applications.

3.2. ^{1}H -Nuclear Magnetic Resonance (NMR) Spectroscopy

The NMR spectra (Figure 2B) evidence the successful methacrylation of gelatin into GelMA. The region "a" at δ = 5.5 ppm corresponds to the protons of the vinyl groups, and peak "b" in the range of δ = 2.8−3.0 ppm corresponds to the protons of amino acid residues such as glycine and proline. Additionally, peak "c" seen at δ = 1.9−2.0 ppm in GelMA corresponds to the methyl protons due to the integration of the methacrylate group in the gelatin backbone.[48] The peak of lysine methylene is observed at 2.9 ppm, which can be used to calculate the DoM of GelMA by determining its area through integral analysis. It was evidenced that the synthesized GelMA shows 74% DoM, indicating a moderate level of methacrylation.

3.3. Ninhydrin Assay

The confirmation of the DoM of GelMA was further validated by the ninhydrin assay (Figure 2D). A standard curve was plotted using various dilutions of gelatin, and the corresponding regression line was determined. The absorbance of the GelMA sample with a nominal concentration of 10 mg/mL was measured and plotted onto the standard curve. Using the linear equation, the apparent gelatin concentration was measured corresponding to GelMA absorbance. Based on the proportion of the remaining free amines, the DoM was calculated to be 65%, confirming the moderate conjugation of methacrylate groups onto the gelatin backbone.[49]

3.4. Spectroscopy Analysis of GelMA

The infrared spectra of the gelatin and GelMA (Figure 2C) illustrate the stretching of O−H resulted in a notable overlapping peak at 3434 cm^{-1} for the major gelatin bands. In gelatin molecules, the characteristic peaks observed at 1642 cm^{-1} and 1547 cm^{-1} correspond to amide I and amide II bands, respectively. The amide I band at 1642 cm^{-1} arises from the C═O stretching vibrations, while the amide II band at 1547 cm^{-1} is attributed to the N−H bending and C−N stretching vibrations.[50] Furthermore, the characteristic absorption bands of GelMA at 1632 cm^{-1}, 1554 cm^{-1}, and 1429 cm^{-1} represent the amide I, II, and III bands, respectively due to the planar vibration of C−N and N−H bonds. Hence, the result evidenced successful synthesis of GelMA, in line with other literature investigations.[51]

3.5. Optimization of SF-GelMA Ink

Various concentrations of GelMA (5−20 w/v %) were mixed with 7.5 w/v % silk fibroin solution and 0.5 w/v % Irgacure 2959 to optimize the formulation of the SF-GelMA ink. An inverse relationship was observed between GelMA concentration and gelation time, with gelation time decreasing from 25 min for 5 w/v % GelMA to 3 min at 20 w/v % GelMA concentration (Table 1). The formulation containing 15 w/v % GelMA demonstrated a gelation time of 8 min, offering an ideal balance between sufficient working time and rapid gelation. Based on this favorable gelation profile, the 7.5 w/v % SF and 15 w/v % GelMA blend was chosen for further characterization. A comprehensive rheological analysis was subsequently performed to evaluate the ink's printability, viscosity profile, and thermal responsiveness.

3.6. Rheological Analysis of SF-GelMA Ink

The rheological performance of SF-GelMA inks composed of 7.5 w/v % silk fibroin and varying GelMA concentrations (10%, 15%, and 20%) was thoroughly evaluated to determine the suitable printability of ink for extrusion-based printing. The temperature-dependent viscosity profiles are presented in Figure 3A. A sharp drop in viscosity was observed around 20−25 °C across all formulations, indicating thermosensitive sol−gel behavior. SF-GelMA 15 (7.5 w/v % SF-15 w/v % GelMA) maintained a moderate viscosity profile with effective gelation time, making it suitable for printing at physiological temperatures. At each formulation (Figure 3B), the viscosity profile was evaluated as a function of shear rate. All the samples demonstrated shear-thinning behavior, which plays a vital role in enabling extrusion-based printing. SF-GelMA 15 ink shows an optimal balance with low viscosity under shear, for smooth extrusion from nozzle, with excellent shape retention after post-printing.

The viscoelastic properties were further evaluated through frequency and temperature sweeps. Figure 3C evidences a higher storage modulus (G') with respect to the loss modulus (G''), and with the increase in GelMA concentration. Gel-like behavior was achieved in SF-GelMA 15 ink. The temperature sweep results are illustrated in Figure 3D, where G' and G'' decrease gradually with rising temperature. Notably, SF-GelMA 15 ink exhibited stable moduli across the physiological range, indicating thermal stability and mechanical reliability post-printing. SF-GelMA 10 (7.5 w/v % SF-10 w/v % GelMA) demonstrated substantially lower storage modulus and viscosity for all conditions, indicating inadequate structural integrity for stable printing. Conversely, SF-GelMA 20 (7.5 w/v % SF-20 w/v % GelMA) was significantly more rigid, which may hinder cell spreading and

Table 1. Effect of GelMA Concentration on Gelation Time in Silk Fibroin Solution

silk	GelMA	gelation time
7.5%	5%	25 min
7.5%	10%	15 min
7.5%	**15%**	**8 min**
7.5%	20%	3 min

https://doi.org/10.1021/acsabm.5c02374
ACS Appl. Bio Mater. XXXX, XXX, XXX−XXX

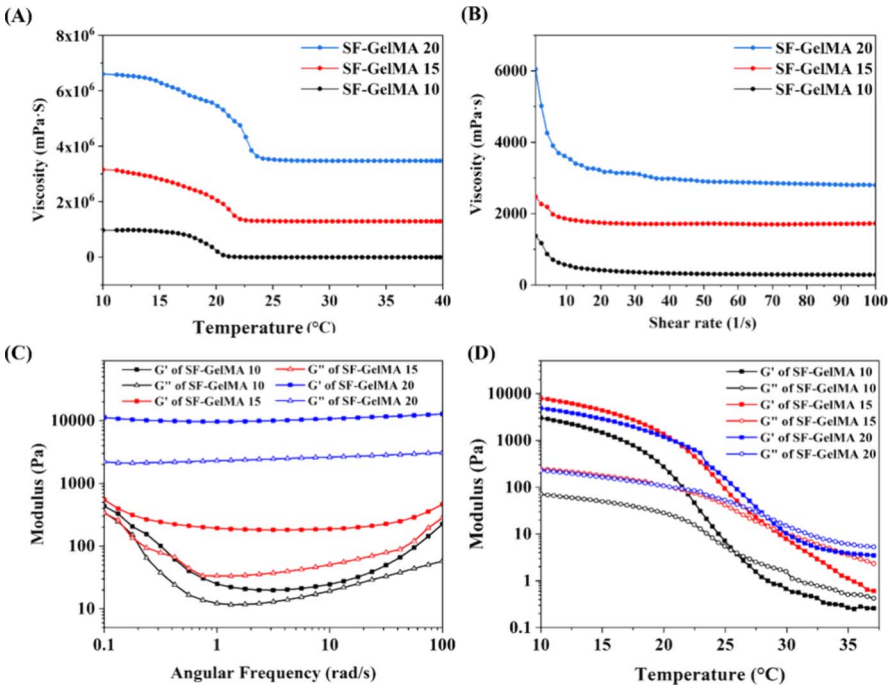

Figure 3. Rheological behavior of the printable ink: (A) viscosity vs temperature profile; (B) viscosity vs shear rate demonstrating shear thinning behavior; thermosensitive sol−gel transition confirmed; (C) angular frequency sweep; (D) temperature sweep showing viscoelastic properties, thermal transitions, and phase changes relevant to the ink printability.

adaptability. Thus, the rheological characteristics justify the selection of SF with 15% GelMA ink as the optimal formulation for further printing applications.

3.7. Design and Fabrication of the 3D Printed Tubular Stent

A precisely designed tubular stent structure was developed using SOLIDWORKS 2020, featuring uniformly distributed circular perforations tailored for vascular tissue engineering applications. The structural details and geometric accuracy are demonstrated in Figure 4A with multiple technical views like sectional, side, top, and isometric. The incorporation of a tubular architecture ensures anatomical conformity and circumferential stress distribution under physiological loading, which is essential to avoid localized stress concentrations that may impair cell viability or matrix remodeling. Following the rheological behavior, a 3D printable construct was fabricated using SF with 15 w/v % GelMA and 0.5 w/v % Irgacure 2959 as the final ink composition. The ink was prepared by thoroughly mixing GelMA into the SF-Irgacure solution under mild heating until complete dissolution was achieved (Figure 4B). The resulting homogenous solution was loaded into a printing syringe to develop the tubular stents based on the optimized design and printing parameters. Post-printed constructs were kept at 4 °C for 2 h to promote initial physical gelation, aiding in the retention of the structural shape. This was followed by chemical crosslinking under UV light, initiating photopolymerization of the GelMA toward a mechanically stable, well-defined tubular construct.

3.8. Physicochemical Characterization of the Tubular Stent

FTIR and XRD analyses were performed for assessing the chemical structure and composition of the developed tubular stent. The FTIR spectra of SF, GelMA, and the SF-GelMA tubular stent are shown in Figure 5A. The characteristic peaks of SF are evident at 1650 cm^{-1} (amide I, C═O stretching), 1537 cm^{-1} (amide II, N−H bending), and 1230 cm^{-1} (amide III, C−N stretching), which confirm the presence of β-sheet and random coil conformations.[52] GelMA exhibits peaks at 3270 cm^{-1} (O−H/N−H stretching), 2945 cm^{-1} (C−H stretching), and 1641 cm^{-1} (amide I), indicating the presence of gelatin in the backbone with successful methacrylation.[49] The presence of amide bands in the stent material confirms the retention of native protein structure, while the C−H and O−H stretching bands indicate the presence of methacrylate groups of GelMA, supporting the formation of a hybrid matrix without significant chemical modification or degradation.

The XRD pattern (Figure 5B) of SF shows a broad peak centered at 21.3°, typically attributed to the semicrystalline β-sheet structure.[53] GelMA displays a broad amorphous peak at 20.5°, consistent with its random-coil conformation.[54] The SF-GelMA tubular stent exhibits diffraction peaks at 20.8°, indicating partial crystallinity due to SF and the amorphous nature contributed by GelMA. The fabricated stent suggests that the incorporation of GelMA into SF may reduce the overall crystallinity while maintaining sufficient structural integrity.

3.9. Mechanical Properties

The mechanical integrity of the SF-GelMA tubular stent was evaluated through uniaxial tensile testing under both dry and wet conditions to simulate handling during implantation and *in vivo* performance. The dry stent exhibited a significantly higher tensile strength of approximately 1.08 MPa with limited elongation (~2%), as seen in Figure 5C, indicating a stiff and brittle nature. However, the wet stent demonstrated a more gradual stress−strain response, with a maximum tensile strength of around 0.45 MPa with a considerably higher elongation

https://doi.org/10.1021/acsabm.5c02374
ACS Appl. Bio Mater. XXXX, XXX, XXX−XXX

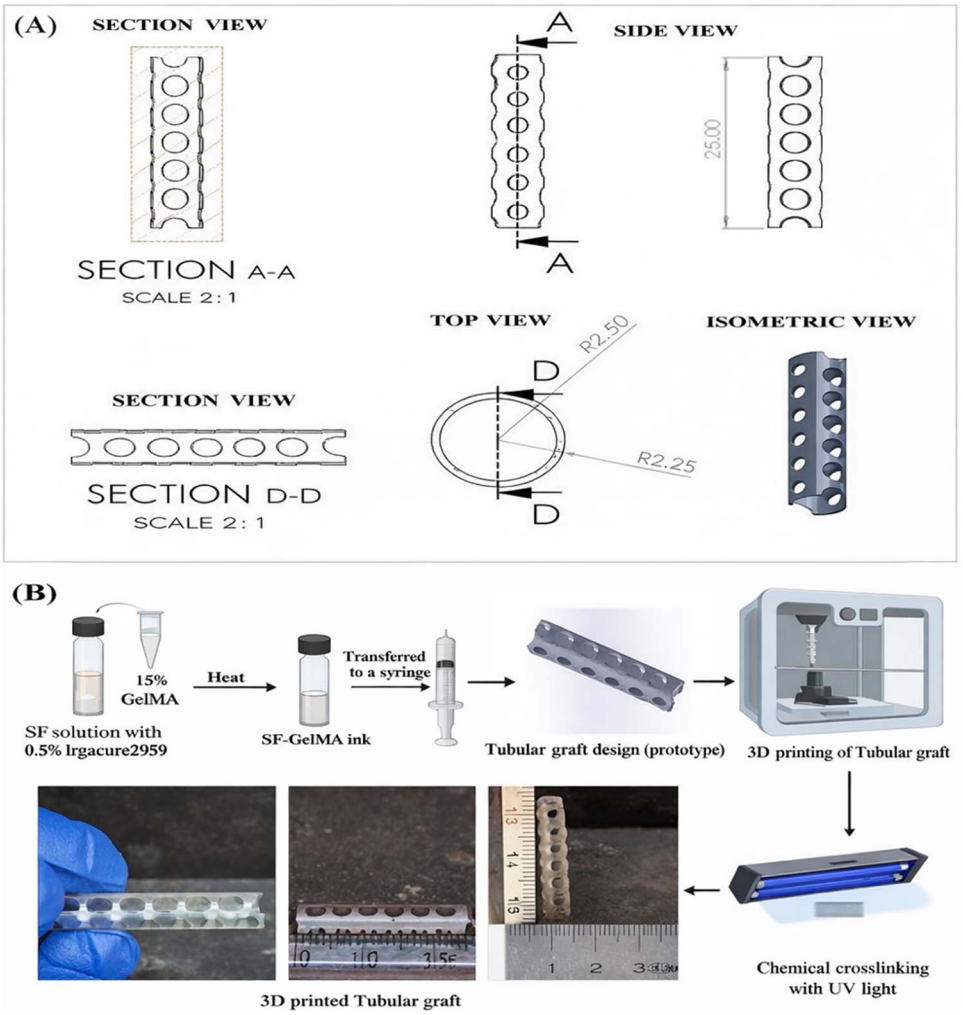

Figure 4. (A) Schematic diagram of the CAD model of the tubular stent; (B) flow diagram of the 3D printing of the tubular stent using SF-GelMA ink.

(~17%) with respect to the stent under the dry condition (Figure 5D). This reflects a more ductile and flexible behavior, attributed to the plasticizing effect of water, which reduces intermolecular bonding and allows for greater deformation before failure. The increase in elasticity of the wet stent is advantageous for mimicking the mechanical compliance of native blood vessels. This balance between strength and flexibility is essential for maintaining structural integrity after post-implantation, supporting its suitability for vascular applications.

3.10. Physical and Morphological Characterization of the Angiogenic Tubular Stent

The structural and surface modifications of the angiogenic tubular stents were comprehensively evaluated using FTIR, X-ray photoelectron spectroscopy (XPS), scanning electron microscopy (SEM), and energy dispersive X-ray (EDX) spectroscopy. FTIR analysis was performed to investigate the chemical functionalities and verify the incorporation of angiogenin into the SF-GelMA tubular stent (Figure 6A). Both SF-GelMA and SF-GelMA-Ang samples exhibited characteristic amide I (~1650 cm^{-1}), amide II (~1540 cm^{-1}), and amide III (~1240 cm^{-1}) bands, showing the proteinaceous nature of the stents. Notably, the SF-GelMA-Ang spectrum displayed distinct shifts and intensity variations in these regions, suggesting molecular interactions between angiogenin and the hydrogel matrix. The deconvoluted FTIR spectra highlight distinct structural variations between SF-GelMA and SF-GelMA-Ang (Figure 6B,C). In the Ang-incorporated system, the amide I region displayed stronger and more defined peaks, reflecting an increased β-sheet content relative to SF-GelMA. This rise in β-sheet structures indicates enhanced molecular ordering and stabilization of the hydrogel network, likely facilitated by angiogenin-mediated interactions. Overall, the results suggest that Ang incorporation promotes a more ordered and structurally robust scaffold.

These spectral changes are indicative of the successful incorporation of angiogenin via covalent bonding through EDC/NHS-mediated crosslinking. XPS was utilized to analyze the elemental composition and chemical state over the stent's surface, as illustrated in Figure 6D,E. Both stents exhibited major peaks corresponding to C 1s, O 1s, and N 1s. However, the SF-GelMA-Ang tubular stent showed a notable increase in the nitrogen content compared to the SF-GelMA tubular stent, consistent with nitrogen enrich angiogenin composition. This result confirms the successful surface functionalization of the stents with angiogenin cues. The surface morphology was assessed by SEM (Figure 6F,H), and the corresponding elemental distribution was confirmed using EDX (Figure 6G,I). The SEM image of the SF-GelMA tubular stent revealed a relatively smooth and

https://doi.org/10.1021/acsabm.5c02374
ACS Appl. Bio Mater. XXXX, XXX, XXX–XXX

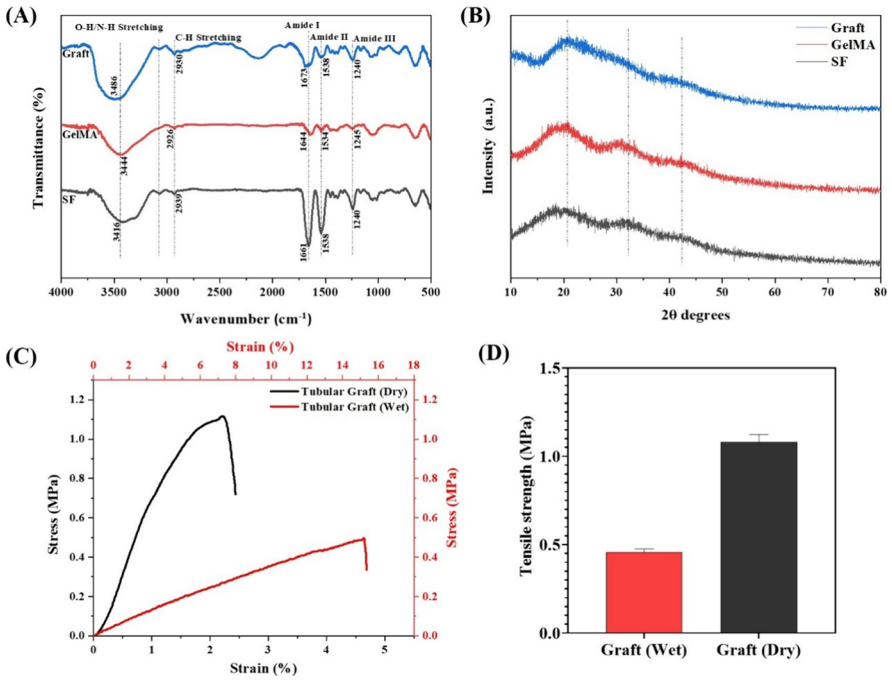

Figure 5. Physicochemical characterization: (A) FTIR spectra confirming the SF/GelMA blend; (B) XRD showing the crystalline structure; UTM shows (C) stress−strain curves; with (D) tensile strength of tubular stents in wet and dry conditions.

homogeneous surface. The SF-GelMA-Ang tubular stent exhibited a rougher texture with microstructural irregularities, potentially enhancing cell attachment and proliferation. EDX spectra validated the presence of angiogenin through a higher nitrogen content in the SF-GelMA-Ang stent.

3.11. Swelling Assay

Swelling behavior critically affects the stent integrity, nutrient diffusion under *in vivo*. The SF-GelMA tubular stent displayed a significantly higher swelling ratio compared to the SF-GelMA-Ang tubular stent (Figure 7A). The SF-GelMA constructs were functionalized with angiogenin using EDC/NHS, enabling covalent amide bond formation between the carboxyl groups of the polymer backbone and the amine groups of angiogenin. This additional chemical modification also increases the effective crosslinking density of GelMA following UV-induced network formation. Significantly, it restricts polymer chain mobility, reduces network mesh size, and results in a more compact matrix structure. This reduced swelling enhances dimensional stability toward vascular applications. The results highlight that the SF-GelMA-Ang tubular stent can exhibit superior structural consistency and long-term suitability, which is particularly important in vascular environments where excessive graft expansion may compromise functionality.

3.12. Protein Adsorption and *In Vitro* Degradation Assay

A time-dependent study of protein adsorption is shown in Figure 7B for both SF-GelMA and SF-GelMA-Ang tubular stents. The SF-GelMA-Ang tubular stent consistently adsorbed significantly higher amounts of protein for all the time points. The increased protein adsorption was observed in the SF-GelMA-Ang tubular stent due to the presence of angiogenic cues that enhance biomolecular interactions over the surface to promote endothelialization, cellular adhesion, proliferation, and tissue remodeling, essential for the successful integration with host tissue. Physiological robustness was assessed by incubating in PBS at 37 °C to confirm the retainability of the geometry and mechanical integrity over time. The degradation of SF-GelMA and SF-GelMA-Ang tubular stents under nonenzymatic and enzymatic conditions over 15 days is shown in Figure 7C,D. The SF-GelMA-Ang tubular stent exhibited lower weight loss than SF-GelMA at different time points in PBS, indicating the slower degradation and better physical stability. The SF-GelMA-Ang tubular stent exhibits improved structural integrity relative to the SF-GelMA composite for greater control over enzymatic degradation, as mediated by pepsin activity.

3.13. Hemocompatibility Assay

Hemocompatibility is the major factor for vascular conduits as it directly comes in contact with blood. The SF-GelMA-Ang tubular stent shows lower hemolysis percentage (~1%) than the SF-GelMA tubular stent (~3%) (Figure 7E) within safe biomedical limits. SEM analysis confirmed optimal RBC morphology (Figure 7F) in the SF-GelMA-Ang tubular stent, while the SF-GelMA tubular stent showed nominal RBC rupture with aggregation, which is not suitable for vascular application. The enhanced blood compatibility of the SF-GelMA-Ang tubular stent is likely due to angiogenic functionalization, which promotes favorable interactions with RBCs, making it suitable for blood-contacting applications in vascular grafting.

3.14. *In Vitro* Cytocompatibility and Morphological Analysis Using L929 Cells

The proliferation of L929 fibroblast cells on the samples was evaluated using the MTT assay over a period of five days, as shown in Figure 8A. Both SF-GelMA and SF-GelMA-Ang samples demonstrated a time-dependent increase in absorbance at 570 nm, indicating the progressive cell proliferation. The cell viability percentage of L929 fibroblasts was further quantified and is presented in Figure 8B. The SF-GelMA-Ang tubular

https://doi.org/10.1021/acsabm.5c02374
ACS Appl. Bio Mater. XXXX, XXX, XXX−XXX

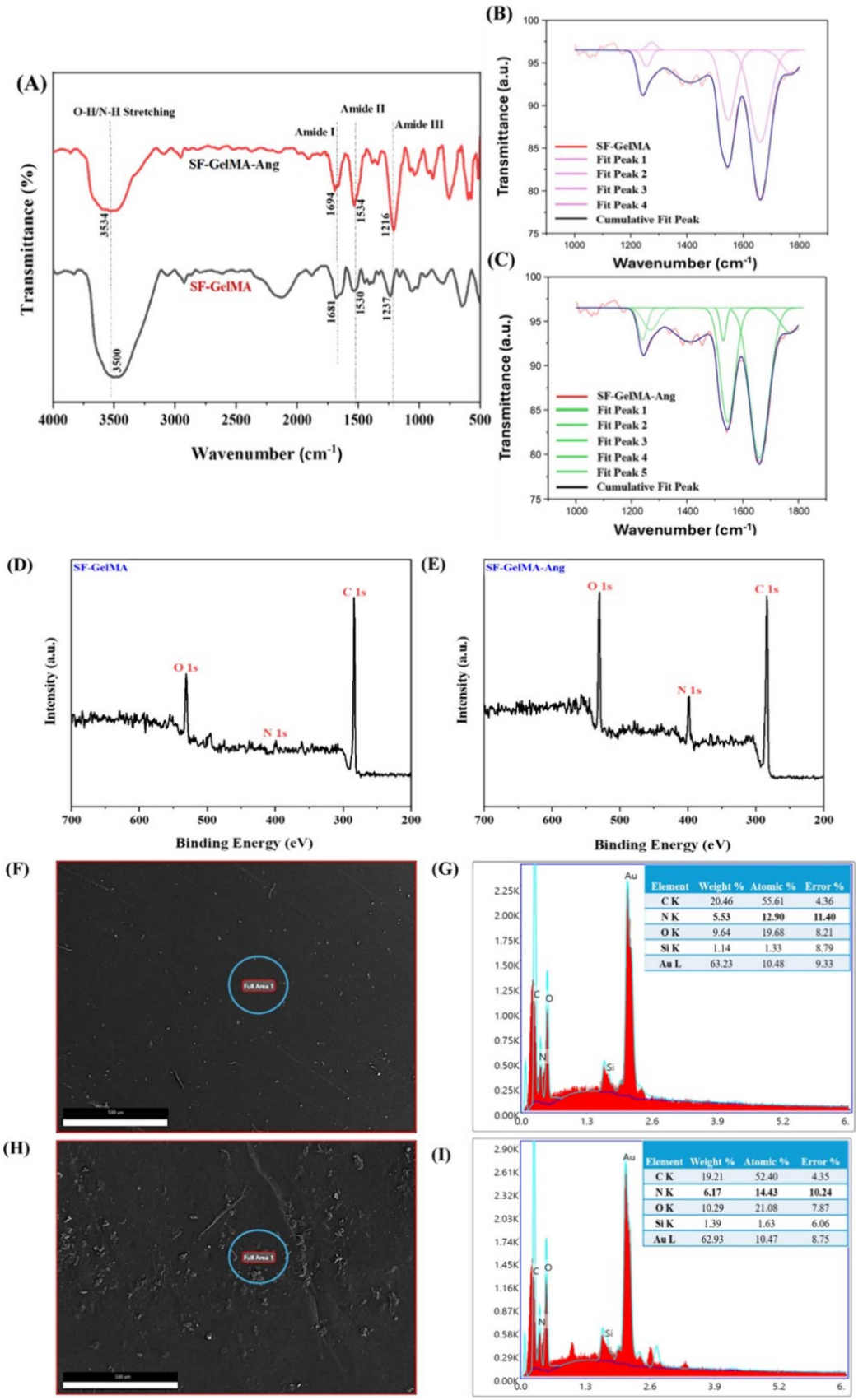

Figure 6. Functional and morphological analysis of stents: (A) FTIR spectra; (B, C) deconvolution of the amide region (1800−1000 cm^{-1}) for the respective SF-GelMA and SF-GelMA-Ang groups; (D, E) XPS analysis confirming angiogenin incorporation; (F−H) FESEM micrographs and (G–I) EDX elemental composition analysis for SF-GelMA and SF-GelMA-Ang tubular stents, respectively.

https://doi.org/10.1021/acsabm.5c02374
ACS Appl. Bio Mater. XXXX, XXX, XXX–XXX

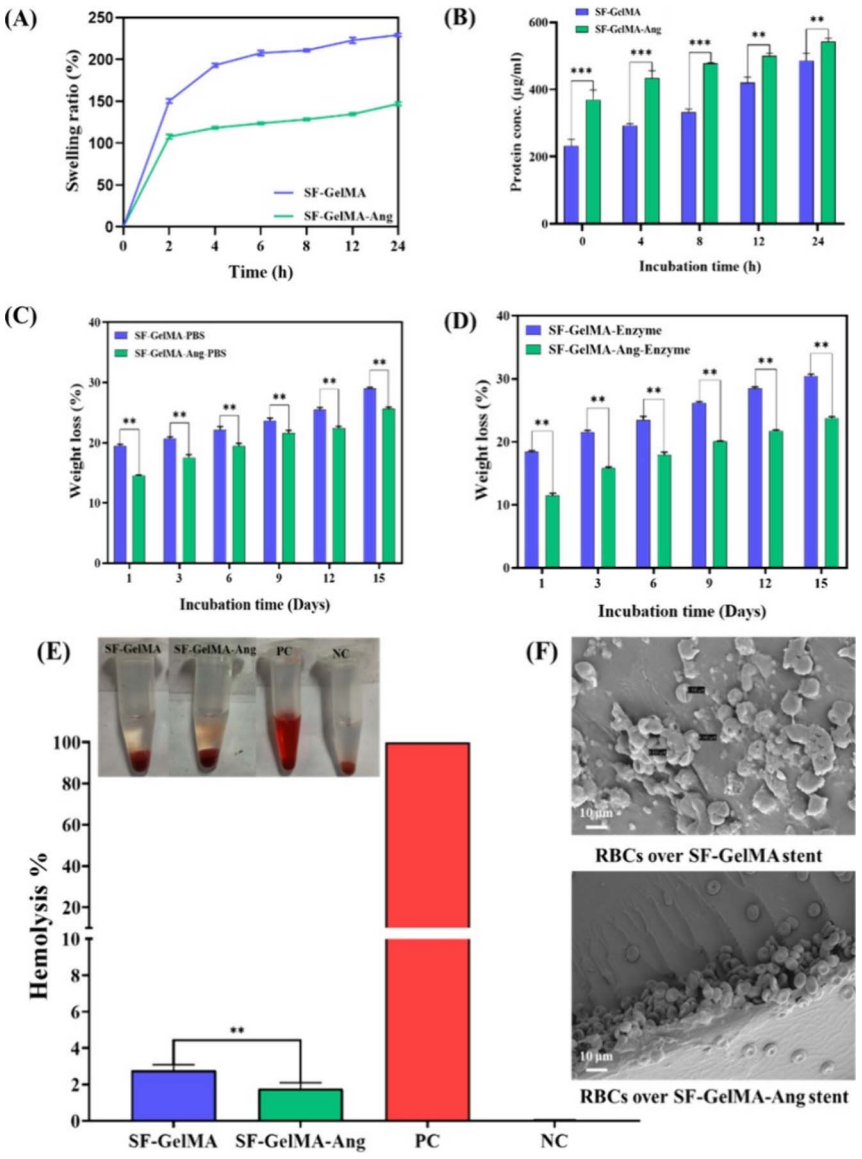

Figure 7. (A) Swelling ratio curve in PBS; (B) protein adsorption for different time points; (C) nonenzymatic and (D) enzymatic degradation in terms of weight loss; (E) hemolysis and (F) SEM micrographs of RBC morphology over the developed SF-GelMA and SF-GelMA-Ang tubular stents.

stents supported a higher percentage of viable cells compared to the unmodified SF-GelMA tubular stent for days 1, 3, and 5.

The viability on SF-GelMA-Ang by day 5 had increased substantially. The cytocompatibility of the stents was further assessed using a Live-Dead assay on L929 fibroblast cells, with results shown in Figure 8C. Fluorescence microscopy images revealed predominantly live cells (green) and a few dead cells (red) for each sample. On day 1, the SF-GelMA-Ang tubular stent exhibited a higher number of attached and viable cells compared to the SF-GelMA tubular stent, indicating improved initial cell adhesion. Both stents show an increase in cell density by day 3. However, the SF-GelMA-Ang tubular stent displayed more uniform and dense cellular coverage. On day 5, the SF-GelMA-Ang tubular stent supported a significantly higher number of viable cells, while the SF-GelMA tubular stent showed moderate cell density with more dead cells.

Overall, observations confirm that angiogenin-modified tubular stents offer superior cytocompatibility and promote enhanced proliferation and viability of L929 fibroblast cells. Hence, the cell viability and cytocompatibility of the samples were assessed through MTT and Live/Dead assays. Further, Rhodamine-DAPI staining images (Figure 8D) demonstrate the time-dependent cellular behavior on the SF-GelMA-Ang tubular stent, where red fluorescence (Rhodamine) marks the actin cytoskeleton and blue (DAPI) stains the nuclei. On day 1, cells appear with elongated morphology, while by day 5, a dense, confluent layer forms with well-developed actin networks, suggesting active proliferation and maturation. Corresponding SEM images confirm progressive cell adhesion and spread over the surface of the SF-GelMA-Ang tubular stent,as depicted in Figure 8E, supporting its potential for vascular tissue engineering.

3.15. *Ex Vivo* Angiogenesis Evaluation Using CAM

The CAM assay was performed to evaluate the angiogenic potential of the developed SF-GelMA and SF-GelMA-Ang tubular stents. The outcomes were analyzed both qualitatively and quantitatively, as depicted in Figure 9. Representative images of the

https://doi.org/10.1021/acsabm.5c02374
ACS Appl. Bio Mater. XXXX, XXX, XXX–XXX

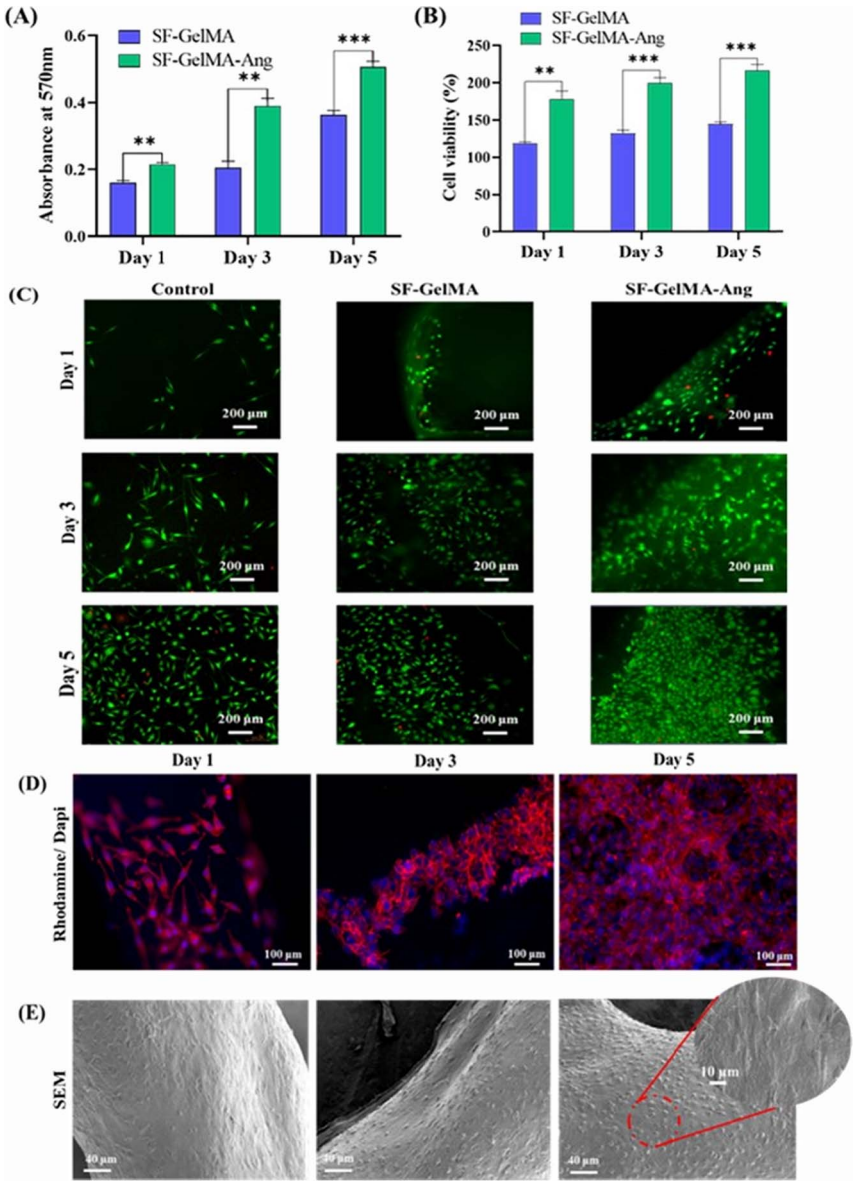

Figure 8. *In vitro* cytotoxicity assessment using the L929 cell line. (A) Absorbance measurement using the MTT assay; (B) cell viability percentage using optical density calculation; (C) Live/Dead fluorescence stain illustrating the cell viability of the SF-GelMA-Ang tubular stent, with respect to control, and SF-GelMA tubular stent; time-dependent morphological analysis of L929 cells on the SF-GelMA-Ang tubular stent using (D) Rhodamine-DAPI staining and (E) SEM imaging showing enhanced cell adhesion and proliferation from day 1 to day 5.

CAMs after 72 h of stent implantation revealed clear differences in neovascularization among the groups (Figure 9A). The control group exhibited sparse and relatively thin blood vessels. CAMs treated with SF-GelMA tubular stents demonstrated a moderate increase in vessel formation and a denser vascular network surrounding the stent zone. The SF-GelMA-Ang group, in comparison, showed a substantial enhancement in blood vessel development, as evidenced by the increased number and complexity of branching vessels radiating from the stent placement region. Quantitative analysis of vessel density was analyzed using ImageJ software. The bar graph (Figure 9B) shows that the vessel density was significantly higher in the SF-GelMA-Ang group compared to both SF-GelMA and control groups. These findings collectively confirm that the addition of the angiogenin factor enhances the neovascular capacity of the SF-GelMA tubular stent, highlighting its potential for vascular tissue engineering applications.

3.16. *In Vivo* Subcutaneous Implantation and Histological Analysis

The tissue compatibility of stents (as marked in a black circle in Figure 10A) were evaluated through subcutaneous implantation in Wistar rats for a period of 3 weeks. Postoperative observation revealed no significant signs of inflammation and scar at the site of implantation. Upon exploration, the stents were found to be well-integrated within the subcutaneous tissue. Greater neovascularization within the implanted area and surrounding tissue was evident at the SF-GelMA-Ang stent (Figure 10C) with respect to the SF-GelMA stent, as illustrated in Figure 10B (as shown in the yellow circle).

https://doi.org/10.1021/acsabm.5c02374
ACS Appl. Bio Mater. XXXX, XXX, XXX–XXX

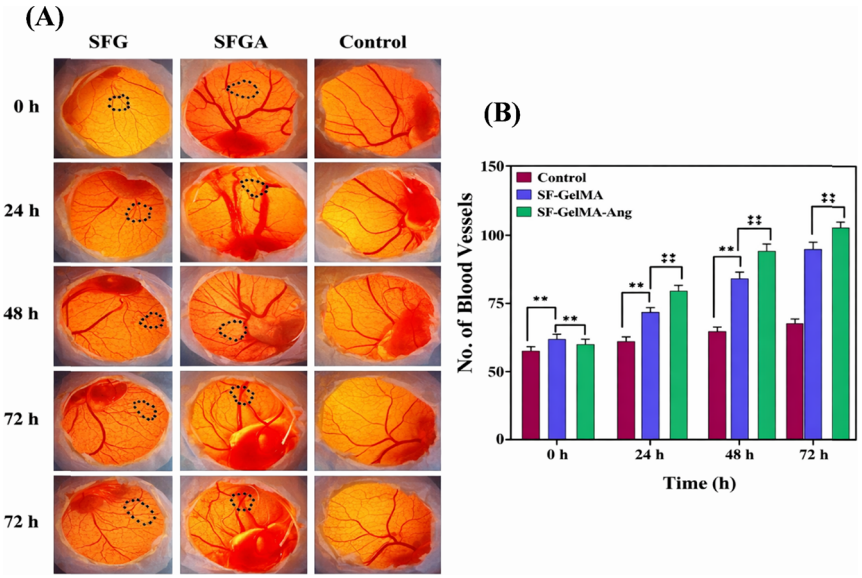

Figure 9. CAM assay results new blood vessel formation after 72 h of treatment with control, SF-GelMA, and SF-GelMA-Ang tubular stents. (A) Representative CAM images with implantation sites marked (blue circles). (B) Quantification of vessel density shows enhanced angiogenesis in the SF-GelMA-Ang group.

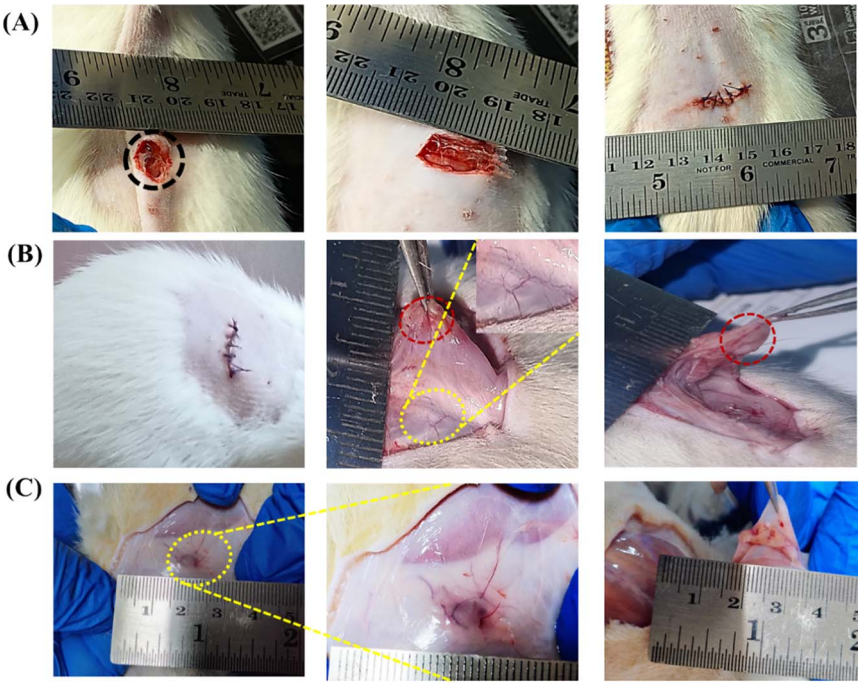

Figure 10. *In vivo* subcutaneous implantation of the stent for soft tissue compatibility assessment: (A) surgical implantation of the stent at the initial day; visualization and stent integration within the retrieved tissue at 21 days of implantation for (B) the SF-GelMA tubular stent and (C) the SF-GelMA-Ang tubular stent.

The histological analysis using H&E and MT staining reveals that tissues from the SF-GelMA-Ang group (Figure 11A–D) exhibit well-organized architecture, dense cellularity, and aligned collagen fibers, indicating effective tissue remodeling and integration. Higher magnification views of deeper tissue planes further highlight organized muscle bundles and fibrous connective tissue with minimal epithelial disruption. In contrast, the SF-GelMA stent (Figure 11E–H) exhibits a disorganized tissue structure and excessive collagen deposition, indicative of poor tissue response. At higher magnification, tissue disorganization, accompanied by chronic inflammatory response and impaired healing progression, was observed. Furthermore, the optical image of the retrieved organs revealed no signs of toxicity or structural abnormalities, confirming that the implanted SF-GelMA-Ang tubular stent is systemically well-tolerated.

All major organs from rats implanted with the SF-GelMA-Ang tubular stent (Figure 11I), including the kidney, heart, lung, spleen, and liver, maintained normal anatomical morphology

https://doi.org/10.1021/acsabm.5c02374
ACS Appl. Bio Mater. XXXX, XXX, XXX–XXX

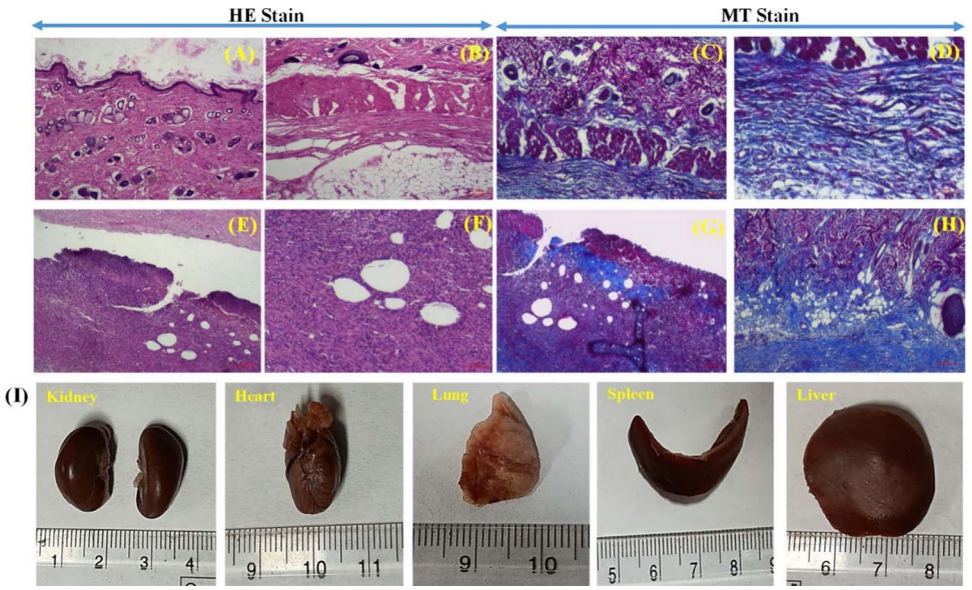

Figure 11. Histological and systemic evaluation of stent biocompatibility: (A, B) H&E and (C, D) MT-stained sections from the SF-GelMA-Ang tubular stent group showing organized tissue architecture and aligned collagen fibers; (E, F) H&E and (G, H) MT-stained sections from the SF-GelMA tubular stent group showing tissue disorganization, excessive collagen deposition, and inflammation; (I) optical images of major organs from the SF-GelMA-Ang tubular stent group showing normal morphology and no signs of macroscopic changes associated with toxicity. Scale bar: A, E, and G - 50 μm; rest - 20 μm.

and size, with no visible indications of inflammation, necrosis, or pathological alterations, collectively demonstrating biocompatibility and nontoxic nature over the 21 day implantation period. Thus, this finding strongly suggests that the material integrates safely within the vascular tissue, without inducing adverse biological responses. These findings demonstrate favorable biocompatibility and angiogenic microenvironment formation, supporting the potential of the SF-GelMA-Ang construct for further evaluation in functional vascular models.

This study presents a comprehensive strategy for developing a bioresorbable, angiogenic tubular stent using SF-GelMA ink via 3D printing, aiming to address existing limitations in stent design and performance. Post rheological analysis evidence that formulation comprising 15 w/v % GelMA and 7.5 w/v % silk fibroin, demonstrating a favorable balance of printability and gelation kinetics that is critical for reliable extrusion-based 3D printing. Functionalization with angiogenin significantly enhanced the stent functioning by increasing protein adsorption, vascularization, and structural stability under physiological conditions compared to the control group. *In vitro* assays confirmed the excellent cytocompatibility of the fabricated SF-GelMA-Ang tubular stents, demonstrating a significant increase in fibroblast viability and sustained proliferation with time, as measured by MTT assays and validated through Live/Dead staining. Additionally, *ex vivo* CAM analysis provided clear evidence of enhanced angiogenic potential, with a pronounced increase in neovascularization and capillary branching around the SF-GelMA-Ang stent site compared to the unmodified stent. *In vivo* subcutaneous implantation in rat models further validated these results by showing robust tissue integration, higher vascular density at the implant interface without any observable signs of systemic toxicity over the implantation period.

In addition to the experimental characterization, computational modeling was performed to further validate the feasibility of protein−matrix interactions at the molecular level. The successful methacrylation of gelatin was confirmed by ^{1}H NMR through the appearance of vinyl proton peaks, while FTIR analysis verified the incorporation of methacryloyl functional groups without disrupting the β-sheet structure of silk fibroin. Rheological studies demonstrated enhanced crosslinking density and mechanical stabilization after EDC/NHS activation, and XPS analysis provided evidence of carbodiimide-mediated amide bond formation on the hydrogel surface. Together, these techniques confirm chemical modification and network formation; however, they do not directly explain whether these modified functional groups can support stable binding of angiogenic proteins. Therefore, molecular docking and dynamics simulations were carried out to assess whether the experimentally verified chemical functionalities, namely, methacryloyl groups and EDC/NHS activated carboxyl sites, can theoretically facilitate stable and energetically favorable interactions with angiogenin and VEGF. The computational results demonstrated consistent binding orientations, strong hydrogen bonding networks, and hydrophobic stabilization, supporting the likelihood of stable protein retention within the activated SF GelMA matrix. Thus, the modeling served as a mechanistic validation step that complements rheological, spectroscopic, and surface analyses, strengthening the correlation between structural modification and biological functionality discussed in this study. These findings highlight the promise of SF-GelMA-Ang tubular stents for applications in vascular tissue engineering applications.

4. CONCLUSIONS

This study proposes a novel strategy for fabricating a customized bioresorbable tubular stent by silk fibroin and GelMA with angiogenin cues through extrusion-based 3D printing techniques. The stents exhibit stable mechanical properties and controlled bioresorbability, addressing key clinical challenges

https://doi.org/10.1021/acsabm.5c02374
ACS Appl. Bio Mater. XXXX, XXX, XXX−XXX

associated with conventional grafting methods and paving the way for biologically passive alternatives. This multifunctional, customized design by wrapping with an electrospun fibrous sheet can be used as small-diameter vascular grafts with enhanced endothelialization, is of non-thrombogenic nature, and promotes localized vascular regeneration. The favorable *in vivo* tissue compatibility and neovascularization further support the grafts' potential for clinical translation in vascular tissue repair and bypass surgeries. Additionally, this innovative technique enables site-specific grafting for cardiac, renal, and other biological conduits, tailored to patient age and activity level. Hence, this research not only addresses critical limitations of current synthetic grafts but also opens new directions for personalized and functionalized grafts in vascular tissue engineering applications.

■ ASSOCIATED CONTENT

Data Availability Statement

The data that support the findings of this study are available from the corresponding author upon reasonable request.

Supporting Information

The Supporting Information is available free of charge at https://pubs.acs.org/doi/10.1021/acsabm.5c02374.

Study of the angiogenin (Ang) release profile: experimental method (DOCX)

Results (MP4)

■ AUTHOR INFORMATION

Corresponding Authors

Sourabh Ghosh – *Department of Textile and Fibre Engineering, Indian Institute of Technology, New Delhi 110016, India;* Email: sourabh.ghosh@textile.iitd.ac.in

Santanu Dhara – *School of Medical Science and Technology, Indian Institute of Technology, Kharagpur, West Bengal 721302, India;* orcid.org/0000-0003-4443-7610; Email: sdhara@smst.iitkgp.ac.in

Authors

Tanutrushna Sahoo – *School of Medical Science and Technology, Indian Institute of Technology, Kharagpur, West Bengal 721302, India; Department of Textile and Fibre Engineering, Indian Institute of Technology, New Delhi 110016, India*

Samir Das – *School of Medical Science and Technology, Indian Institute of Technology, Kharagpur, West Bengal 721302, India*

Sheeba Sonali – *School of Medical Science and Technology, Indian Institute of Technology, Kharagpur, West Bengal 721302, India*

Sayan Mukherjee – *School of Medical Science and Technology, Indian Institute of Technology, Kharagpur, West Bengal 721302, India; School of Nanoscience and Technology, Indian Institute of Technology, Kharagpur, West Bengal, 721302, India*

Nantu Dogra – *School of Medical Science and Technology, Indian Institute of Technology, Kharagpur, West Bengal 721302, India*

Chandrashish Roy – *Department of Textile and Fibre Engineering, Indian Institute of Technology, New Delhi 110016, India*

Radha Prabhu K – *B C Roy Technology Hospital, Indian Institute of Technology Kharagpur, Kharagpur, West Bengal 721302, India School of Nanoscience and Technology, Indian Institute of Technology, Kharagpur, West Bengal, 721302, India Equally Contributed*

Complete contact information is available at: https://pubs.acs.org/doi/10.1021/acsabm.5c02374

Author Contributions

#T.S. and S.Das contributed equally. T.S. and S.Das: Fabrication, characterization, mechanical testing, biological assay, draft preparation. S.S.: Methodology, data curation, *in vitro* study. S.M.: *Ex vivo* and angiogenic study. N.D.: *In vitro* and *in vivo* study. C.R.: Computational modeling analysis. R.P.K.: *In vivo* and hemocompatibility study. S.G. and S.Dhara: Conceptualization, study design, manuscript finalization, and correction.

Notes

The authors declare no competing financial interest.

■ ACKNOWLEDGMENTS

The authors express their gratitude to the Indian Council of Medical Study (ICMR, Grant Number: 2020-4833) and the Ministry of Education (MOE) for their financial support in conducting this study. The authors express their gratitude to the Institutional Animal Ethics Committee of IIT Kharagpur, CRF, IIT Kharagpur, and all the Biomaterials and Tissue Engineering (BMTE) members in the lab.

■ REFERENCES

(1) Şahin, B.; İlgün, G. Risk factors of deaths related to cardiovascular diseases in World Health Organization (WHO) member countries. *Health Soc. Care Community* **2022**, *30* (1), 73–80.

(2) Tousoulis, D.; Kampoli, A. M.; Papageorgiou, N.; Androulakis, E.; Antoniades, C.; Toutouzas, K.; Stefanadis, C. Pathophysiology of atherosclerosis: the role of inflammation. *Curr. Pharm. Des.* **2011**, *17* (37), 4089–4110.

(3) Krings, T.; Mandell, D. M.; Kiehl, T. R.; Geibprasert, S.; Tymianski, M.; Alvarez, H.; Terbrugge, K. G.; Hans, F. J. Intracranial aneurysms: from vessel wall pathology to therapeutic approach. *Nat. Rev. Neurol.* **2011**, *7* (10), 547–559.

(4) Rozen, W. M.; Ye, X.; Guio-Aguilar, P. L.; Alonso-Burgos, A.; Goldblatt, J.; Ashton, M. W.; Whitaker, I. S. Autologous microsurgical breast reconstruction and coronary artery bypass grafting: an anatomical study and clinical implications. *Breast Cancer Res. Treat.* **2012**, *134*, 181–198.

(5) Obiweluozor, F. O.; Emechebe, G. A.; Kim, D. W.; Cho, H. J.; Park, C. H.; Kim, C. S.; Jeong, I. S. Considerations in the development of small-diameter vascular graft as an alternative for bypass and reconstructive surgeries: a review. *Cardiovasc. Eng. Technol.* **2020**, *11*, 495–521.

(6) Grines, C. L.; Cox, D. A.; Stone, G. W.; Garcia, E.; Mattos, L. A.; Giambartolomei, A.; Brodie, B. R.; Madonna, O.; Eijgelshoven, M.; Lansky, A. J.; O'Neill, W. W. Coronary angioplasty with or without stent implantation for acute myocardial infarction. *N. Engl. J. Med.* **1999**, *341* (26), 1949–1956.

(7) Hermawan, H.; Dubé, D.; Mantovani, D. Developments in metallic biodegradable stents. *Acta Biomater.* **2010**, *6* (5), 1693–1697.

(8) Gupta, P.; Mandal, B. B. Tissue-engineered vascular grafts: emerging trends and technologies. *Adv. Funct. Mater.* **2021**, *31* (33), No. 2100027.

(9) Van Damme, H.; Deprez, M.; Creemers, E.; Limet, R. Intrinsic structural failure of polyester (Dacron) vascular grafts: a general review. *Acta Chir. Belg.* **2005**, *105* (3), 249–255.

(10) Cassady, A. I.; Hidzir, N. M.; Grøndahl, L. Enhancing expanded poly(tetrafluoroethylene) (ePTFE) for biomaterials applications. *J. Appl. Polym. Sci.* **2014**, *131* (15), No. 40533.
(11) Hiob, M. A.; She, S.; Muiznieks, L. D.; Weiss, A. S. Biomaterials and modifications in the development of small-diameter vascular grafts. *ACS Biomater. Sci. Eng.* **2017**, *3* (5), 712–723.
(12) Rob, C. Vascular surgery. In *Modern Trends in Surgical Materials*; Gillis, L., Butterworths: London, **1958**, 175−185.
(13) Sauvage, L. R.; Berger, K. E.; Mansfield, P. B.; Wood, S. J.; Smith, J. C.; Overton, J. B. Future directions in the development of arterial prostheses for small and medium caliber arteries. *Surg. Clin. North Am.* **1974**, *54* (1), 213–228.
(14) Wang, X.; Lin, P.; Yao, Q.; Chen, C. Development of small-diameter vascular grafts. *World J. Surg.* **2007**, *31* (4), 682–689.
(15) Takagi, H.; Goto, S. N.; Matsui, M.; Manabe, H.; Umemoto, T. A contemporary meta-analysis of Dacron versus polytetrafluoroethylene grafts for femoropopliteal bypass grafting. *J. Vasc. Surg.* **2010**, *52* (1), 232–236.
(16) Fathi-Karkan, S.; Banimohamad-Shotorbani, B.; Saghati, S.; Rahbarghazi, R.; Davaran, S. A critical review of fibrous polyurethane-based vascular tissue engineering scaffolds. *J. Biol. Eng.* **2022**, *16* (1), 6.
(17) Gorman, S. P.; Jones, D. S.; Bonner, M. C.; Akay, M.; Keane, P. F. Mechanical performance of polyurethane ureteral stents in vitro and ex vivo. *Biomaterials* **1997**, *18* (20), 1379–1383.
(18) Patel, H. N.; Thai, K. N.; Chowdhury, S.; Singh, R.; Vohra, Y. K.; Thomas, V. In vitro degradation and cell attachment studies of electrospun polymeric tubular grafts. *Prog. Biomater.* **2015**, *4*, 67–76.
(19) Jansen, K.; Castilho, M.; Aarts, S.; Kaminski, M. M.; Lienkamp, S. S.; Pichler, R.; Malda, J.; Vermonden, T.; Jansen, J.; Masereeuw, R. Fabrication of kidney proximal tubule grafts using biofunctionalized electrospun polymer scaffolds. *Macromol. Biosci.* **2019**, *19* (2), No. 1800412.
(20) Shahverdi, M.; Seifi, S.; Akbari, A.; Mohammadi, K.; Shamloo, A.; Movahhedy, M. R. Melt electrowriting of PLA, PCL, and composite PLA/PCL scaffolds for tissue engineering application. *Sci. Rep.* **2022**, *12* (1), 19935.
(21) Min, S.; Gao, X.; Liu, L.; Tian, L.; Zhu, L.; Zhang, H.; Yao, J. Fabrication and characterization of porous tubular silk fibroin scaffolds. *J. Biomater. Sci. Polym. Ed.* **2009**, *20* (13), 1961–1974.
(22) Marelli, B.; Achilli, M.; Alessandrino, A.; Freddi, G.; Tanzi, M. C.; Farè, S.; Mantovani, D. Collagen-reinforced electrospun silk fibroin tubular construct as small calibre vascular graft. *Macromol. Biosci.* **2012**, *12* (11), 1566–1574.
(23) Catto, V.; Farè, S.; Cattaneo, I.; Figliuzzi, M.; Alessandrino, A.; Freddi, G.; Remuzzi, A.; Tanzi, M. C. Small diameter electrospun silk fibroin vascular grafts: mechanical properties, in vitro biodegradability, and in vivo biocompatibility. *Mater. Sci. Eng., C* **2015**, *54*, 101–111.
(24) Soffer, L.; Wang, X.; Zhang, X.; et al. Silk-based electrospun tubular scaffolds for tissue-engineered vascular grafts. *J. Biomater. Sci., Polym. Ed.* **2008**, *19*, 653–664.
(25) Altman, G. H.; Diaz, F.; Jakuba, C.; et al. Silk-based biomaterials. *Biomaterials* **2003**, *24*, 401–416.
(26) Wang, Y.; Kankala, R. K.; Zhu, K.; Wang, S. B.; Zhang, Y. S.; Chen, A. Z. Coaxial extrusion of tubular tissue constructs using a gelatin/GelMA blend bioink. *ACS Biomater. Sci. Eng.* **2019**, *5*, 5514–5524.
(27) Xiao, W.; He, J.; Nichol, J. W.; Wang, L.; Hutson, C. B.; Wang, B.; et al. Synthesis and characterization of photocrosslinkable gelatin and silk fibroin interpenetrating polymer network hydrogels. *Acta Biomater.* **2011**, *7*, 2384–2393.
(28) Bhat, S. M.; Badiger, V. A.; Vasishta, S.; Chakraborty, J.; Prasad, S.; Ghosh, S.; Joshi, M. B. 3D tumor angiogenesis models: recent advances and challenges. *J. Cancer Res. Clin. Oncol.* **2021**, *147*, 3477–3494.
(29) Ghosh, S.; Joshi, M. B.; Ivanov, D.; Feder-Mengus, C.; Spagnoli, G. C.; Martin, I.; Erne, P.; Resink, T. J. Use of multicellular tumor spheroids to dissect endothelial cell−tumor cell interactions: a role for T-cadherin in tumor angiogenesis. *FEBS Lett.* **2007**, *581*, 4523–4528.
(30) Xiao, S.; et al. Gelatin methacrylate (GelMA)-based hydrogels for cell transplantation: an effective strategy for tissue engineering. *Stem Cell Rev. Rep.* **2019**, *15*, 664–679.
(31) Tutar, R.; et al. Photocurable silk fibroin-based tissue sealants with enhanced adhesive properties for the treatment of corneal perforations. *J. Mater. Chem. B* **2022**, *10*, 4223–4234.
(32) Jahani, M.; Rezazadeh, D.; Mohammadi, P.; Abdolmaleki, A.; Norooznezhad, A.; Mansouri, K. Regenerative medicine and angiogenesis: challenges and opportunities. *Adv. Pharm. Bull.* **2020**, *10*, 490–498.
(33) Mahaling, B.; Roy, C.; Ghosh, S. Silk−gelatin hybrid hydrogel: a potential carrier for RNA therapeutics. *J. Mater. Chem. B* **2024**, *12*, 6203–6220.
(34) Majumder, N.; Roy, C.; Doenges, L.; Martin, I.; Barbero, A.; Ghosh, S. Covalent conjugation of small molecule inhibitors and growth factors to a silk fibroin-derived bioink to develop phenotypically stable 3D bioprinted cartilage. *ACS Appl. Mater. Interfaces* **2024**, *16*, 9925–9943.
(35) Kuo, C. Y.; Guo, T.; Cabrera-Luque, J.; Arumugasaamy, N.; Bracaglia, L.; Garcia-Vivas, A.; Santoro, M.; Baker, H.; Fisher, J.; Kim, P. Placental basement membrane proteins are required for effective cytotrophoblast invasion in a three-dimensional bioprinted placenta model. *J. Biomed. Mater. Res., Part A* **2018**, *106* (6), 1476–1487.
(36) Dubey, P.; Murab, S.; Karmakar, S.; Chowdhury, P. K.; Ghosh, S. Modulation of self-assembly process of fibroin: an insight for regulating the conformation of silk biomaterials. *Biomacromolecules* **2015**, *16*, 3936–3944.
(37) Zatorski, J. M.; Montalbine, A. N.; Ortiz-Cárdenas, J. E.; Pompano, R. R. Quantification of fractional and absolute functionalization of gelatin hydrogels by optimized ninhydrin assay and 1H NMR. *Anal. Bioanal. Chem.* **2020**, *412* (24), 6211–6220.
(38) Lee, B. H.; Shirahama, H.; Cho, N. J.; Tan, L. P. Efficient and controllable synthesis of highly substituted gelatin methacrylamide for mechanically stiff hydrogels. *RSC Adv.* **2015**, *5*, 106094–106097.
(39) Shukla, P.; Mitruka, M.; Pati, F. The effect of the synthetic route on the biophysiochemical properties of methacrylated gelatin (GelMA)-based hydrogel for development of GelMA-based bioinks for 3D bioprinting applications. *Materialia* **2022**, *25*, No. 101542.
(40) Vijayaraghavan, R.; Loganathan, S.; Valapa, R. B. 3D bioprinted photocrosslinkable GelMA/methylcellulose hydrogel mimicking native corneal model with enhanced in vitro cytocompatibility and sustained keratocyte phenotype for stromal regeneration. *Int. J. Biol. Macromol.* **2024**, *264*, No. 130472.
(41) Yan, M.; An, X.; Jiang, Z.; Duan, S.; Wang, A.; Zhao, X.; Li, Y. Effects of cross-linking with EDC/NHS and genipin on characterizations of self-assembled fibrillar gel prepared from tilapia collagen and alginate. *Polym. Degrad. Stab.* **2022**, *200*, No. 109929.
(42) Theron, J. P.; Knoetze, J. H.; Sanderson, R. D.; Hunter, R.; Mequanint, K.; Franz, T.; Zilla, P.; Bezuidenhout, D. J. Modification, crosslinking and reactive electrospinning of a thermoplastic medical polyurethane for vascular graft applications. *Acta Biomater.* **2010**, *6*, 2434–2447.
(43) Bankoti, K.; Rameshbabu, A. P.; Datta, S.; Maity, P. P.; Goswami, P.; Datta, P.; Ghosh, S. K.; Mitra, A.; Dhara, S. Accelerated healing of full thickness dermal wounds by macroporous waterborne polyurethane-chitosan hydrogel scaffolds. *Mater. Sci. Eng., C* **2017**, *81*, 133–143.
(44) Evans, B. C.; Nelson, C. E.; Shann, S. Y.; Beavers, K. R.; Kim, A. J.; Li, H.; Nelson, H. M.; Giorgio, T. D.; Duvall, C. L. Ex vivo red blood cell hemolysis assay for the evaluation of pH-responsive endosomolytic agents for cytosolic delivery of biomacromolecular drugs. *J. Visualized Exp.* **2013**, *73*, No. e50166.
(45) Das, S.; Rana, M.; Prabhu, R. K.; Jana, S.; Dogra, N.; Reddy, K. P.; Chowdhury, A. R.; Datta, P.; Bagade, A.; Fulzele, P.; Zahiruddin, Q. Bioresorbable-bioactive auxetic "personalised" phalanx with a CT-guided AI-driven model towards in vivo prediction of bone regeneration. *Biomater. Sci.* **2026**, *14*, 571–587.
(46) Tseng, Y. C.; Roan, J. N.; Ho, Y. C.; Lin, C. C.; Yeh, M. L. An in vivo study on endothelialized vascular grafts produced by autologous biotubes and adipose stem cells (ADSCs). *J. Mater. Sci.: Mater. Med.* **2017**, *28* (10), 166.
(47) Ojha, A. K.; Rajasekaran, R.; Hansda, A. K.; Singh, A.; Dutta, A.; Seesala, V. S.; Das, S.; Dogra, N.; Sharma, S.; Goswami, R.; Chaudhury, K. Biodegradable multi-layered silk fibroin-PCL stent for the

https://doi.org/10.1021/acsabm.5c02374
ACS Appl. Bio Mater. XXXX, XXX, XXX−XXX

management of cervical atresia: in vitro cytocompatibility and extracellular matrix remodeling in vivo. *ACS Appl. Mater. Interfaces* **2023**, *15* (33), 39099–39116.

(48) Modaresifar, K.; Hadjizadeh, A.; Niknejad, H. Design and fabrication of GelMA/chitosan nanoparticles composite hydrogel for angiogenic growth factor delivery. *Artif. Cells Nanomed. Biotechnol.* **2018**, *46*, 1799–1808.

(49) Zhou, L.; Tan, G.; Tan, Y.; Wang, H.; Liao, J.; Ning, C. Biomimetic mineralization of anionic gelatin hydrogels: effect of degree of methacrylation. *RSC Adv.* **2014**, *4*, 21997–22008.

(50) Sun, M.; Sun, X.; Wang, Z.; Guo, S.; Yu, G.; Yang, H. Synthesis and properties of gelatin methacryloyl (GelMA) hydrogels and their recent applications in load-bearing tissue. *Polymers* **2018**, *10*, 1290.

(51) Saleki, A.; et al. An injectable nanocomposite IPN hydrogel based on gelatin methacrylate/alginate/COF for tissue engineering applications. *Macromol. Mater. Eng.* **2024**, *309*, No. 2300417.

(52) Kim, S. H.; Nam, Y. S.; Lee, T. S.; Park, W. H. Silk fibroin nanofiber: electrospinning, properties, and structure. *Polym. J.* **2003**, *35*, 185–190.

(53) Wang, H. Y.; Zhang, Y. Q. Effect of regeneration of liquid silk fibroin on its structure and characterization. *Soft Matter* **2013**, *9*, 138–145.

(54) Chen, S.; Wang, Y.; Lai, J.; Tan, S.; Wang, M. Structure and properties of gelatin methacryloyl (GelMA) synthesized in different reaction systems. *Biomacromolecules* **2023**, *24*, 2928–2941.

https://doi.org/10.1021/acsabm.5c02374
ACS Appl. Bio Mater. XXXX, XXX, XXX–XXX